ORIGINAL RESEARCH

Novel fluorinated pyrazole-based heterocycles scaffold: cytotoxicity, in silico studies and molecular modelling targeting double mutant EGFR [L858R/T790M] as antiproliferative and apoptotic agents

Eman A. Fayed [1] · Nirvana A. Gohar[2] · Ashraf H. Bayoumi[3] · Yousry A. Ammar[4]

Abstract

Hepatocellular carcinoma (HCC), also known as hepatoma, is the most prevalent type of primary liver cancer. It begins in the hepatocytes, the liver's major cell type. Cancer that began in another region of the body but has spread to the liver is known as secondary cancer of life; several still unmet demands for better, less toxic therapy to treat this malignant tumor. Several novel pyrazolo[1,5-*a*]pyrimidine derivatives were synthesized as part of our goal to develop promising anticancer drugs. All the synthesized hybrids have been screened for their cytotoxicity effect against three cancer cell lines which are; HepG-2, HCT-116, and MCF-7. The liver cancer cells were found to be the most sensitive to the effect of the new molecules. A subsequent set of in vitro biological evaluation studies has been conducted on the most promising derivatives to identify their effect on such a cancer type. In HepG-2 cells, four derivatives (**8a**, **8b**, **10c**, and **11b**) demonstrated good anticancer activity. The most efficacious compounds were **8b** and **10c**, which had IC$_{50}$ values of 2.36 ± 0.14 and $1.14 \pm 0.063 \, \mu M$, respectively, higher than the reference medication Imatinib. The latter's putative molecular effect has been investigated further by looking at its influence on the cell cycle, EGFR, and specific apoptotic and anti-apoptotic markers in HepG-2 cells. These findings indicated that **8b** and **10c** could trigger apoptosis by upregulating BAX and caspase-3 and cell cycle at the Pre-G1 and G2-M stages. The compounds **8b** and **10c** showed high potency for EGFR with IC$_{50}$ equal to 0.098 and 0.079 μM, respectively. Compound **10c** had the most effective inhibitory activity for EGFR [L858R-TK] with IC$_{50}$ (36.79 nM). Additionally, in silico ADMET and docking studies were done for the most active hits, representing good results.

✉ Eman A. Fayed
  alfayed_e@azhar.edu.eg

1 Pharmaceutical Organic Chemistry Department, Faculty of Pharmacy (Girls), Al-Azhar University, Cairo 11754, Egypt

2 Department of Pharmaceutical Organic Chemistry, Faculty of Pharmacy, MTI University, Cairo, Egypt

3 Pharmaceutical Organic Chemistry Department, Faculty of Pharmacy (Boys), Al-Azhar University, Cairo 11884, Egypt

4 Chemistry Department, Faculty of Science (Boys), Al-Azhar University, Cairo 11884, Egypt

Medicinal Chemistry Research (2023) 32:369–388

Graphical Abstract

Novel Fluorinated Pyrazole-Based Heterocycles Scaffold: Cytotoxicity, In Silico Studies and Molecular Modelling Targeting Double Mutant EGFR [L858R/T790M] as Antiproliferative and Apoptotic Agents
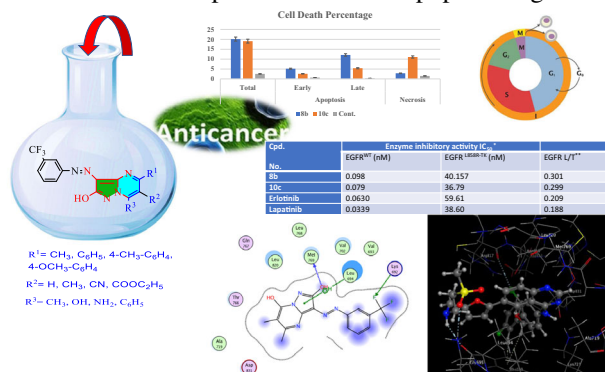
Keywords Fluorinated-pyrazole · Pyrazolo-pyrimidines · Anticancer activity · Apoptosis · In silico ADMET studies · Molecular modeling

Introduction

Cancer has gradually become a major threat to human health with ecological changes and environmental deterioration [1–4]. Cancer is one of the degenerative conditions of rodents and people because of age [5–7]. A balance between cellular proliferation, distinguishing, and apoptosis is organized in physiological processes [8]. Cell death is a programmed process that can be enhanced through DNA-damaging drugs such as chemotherapeutic substances and radiation; apoptosis is a dynamic process. In recent studies, a good relationship has been shown between increased resistance to cancer medicines and decreased apoptosis [9]. Therefore, apoptosis is a major determinant of anticancer therapy responsiveness [10]. Apoptosis suppression is therefore supposed to play an important role in cancer progression during the entire course of carcinogenesis [11, 12]. BAX is a humanly encrypted protein called the Bcl-2-like protein 4, used in apoptosis-regulating systems. It is also a member of the Bcl-2 gene families, which may make hetero- or homo-dimers and act as anti- or pro-apoptotic regulatory bodies involved in a wide range of cellular activities [13, 14]. This protein is the heterodimer with Bcl-2, which functions as an apoptotic activator.

Caspase 3 is the most important protein in the caspase family that is highly conserved and functions as a central apoptosis regulator in multicellular organisms. Thus, it has become an attractive strategy for the treatment of cancer in critical regulators of apoptosis to induce apoptosis in cancer cells [11, 15–19]. The molecular mechanisms used by cancer cells for apoptosis are multifarious [20]. They acquire apoptosis resistance through the expression of anti-apoptotic proteins like Bcl-2, or the down-regulation of various caspases and pro-apoptotic proteins like BAX [21]. A significant determinant of cell survival is the relationship between pro-apoptotic and anti-apoptotic levels [22].

In addition, the Epidermal Growth Factor (EGFR) receptor, which is overexpressed by many cancer cells, such as (breasts, ovaries, and the human colon) is a transmembranous glycoprotein tyrosine kinase receptor [23]. The overexpression of the EGFR family leads to multiple tyrosine residues being auto-phosphorylated within a COOH terminal waist receptor and to some cell proliferation, differentiation, and anti-apoptosis storm. Therefore, an important role in the development of targeted chemical therapeutic agents was found in the inhibition of the EGFR family [23–25]. The anticancer agents currently suffer from various adverse effects associated with drugs and/or multidrug resistance to tumors [26–28] in clinical cases. One of the strategies to solve this problem is to discover new molecules with high-potential cancer activities with rapidly growing multidrug resistance.

Moreover, pyrazolo-pyrimidines are rigid heterocycles that have recently emerged as animated building blocks for pharmaceuticals. Due to their broad potential biological and chemotherapeutic activities, organic chemists have been attracted by pyrazolo-pyrimidine derivatives in recent years. Pyrazolo-pyrimidine's biological activities include anxiolytic [29], tuberculostatic [30], neuroleptic [31], benzodiazepine receptor ligands [32], antimalarial, antioxidant [33], and antifungal effects [34]. Also, they appeared in many significant bioactivities such as anti-inflammatory [35], anticancer [36–41], and antimicrobial [42].

🄯 Springer

Fluorine-containing building blocks are also significant since they are commonly used in the production of medications across a wide range of therapeutic applications [43]. The trifluoromethyl group, which is one of the most lipophilic groups, has several dramatic consequences on the pharmacological properties of the molecule [44–48]. It simplifies the absorption of fluorinated molecules into cell membranes, improving selectivity, effectiveness, and bioavailability [49]. The inclusion of the azo group has also been shown to improve the biological activity of heterocyclic compounds [50–52]. Developing novel analogs based on established inhibitors is a significant way of detecting new anticancer medications with great efficiency, as is using a pharmacophore hybridization approach for synthesizing new bioactive chemicals in modern medicinal chemistry.

Depending on the previous results and in continuation of our previous efforts in designing new heterocyclic compounds having biological activity [53–59]. Based on the aforementioned data regarding the biological significance of both pyrazolo-pyrimidines, Fluorine, and azo group moieties, it was conceptualized that the tethering of these pharmacophores in one scaffold using a fragment-based drug design approach would be of great interest to develop highly potent anticancer agents.

As a result, we reported the design and synthesis of new pyrazoles and pyrazolopyrimidines with trifluoromethyl and azo moieties attached to their molecular framework to investigate the influence of such a connection on anticancer activity and cytotoxicity in the new materials. The effect of mitochondrial apoptosis pathway BAX and Bcl-2 proteins were next studied, followed by kinases assays such as EGFR in both wild type and mutant type, cell cycle progression to examine the mode of action, and finally in silico analysis such as molecular docking and ADMET was performed (Fig. 1).

Discussion

Chemistry

In the current work, the procedures described in Schemes 1–3 were used to synthesize the target hybrids.

According to the literature, the initial chemical, 3-trifluoro aniline, was diazotized and then linked with ethyl cyanoacetate while sodium acetate was present [60].

The IR spectra of compound **3** revealed a peak at 3218 attributable to NH and a distinct peak of the $C≡N$ group at $2219 \, cm^{-1}$, confirming the structure of the molecule. In the ^1H NMR, triplet and quartet signals for CH_3 and CH_2-ester appeared at δ 1.26 and 4.26 ppm, respectively, as well as a single new D_2O exchangeable peak for NH proton at δ 12.38 ppm.

3-Hydroxy pyrazole derivatives **4a&b** were prepared through the reaction of hydrazono-ethyl cyanoacetate with hydrazine hydrate [61] and phenyl-hydrazine via reflux in ethanol.

Based on elemental and spectral data, the proposed structures of compounds **4a** and **b** were verified. Strong absorption bands at 3403, 3326, and $3128 \, cm^{-1}$, which correspond to the OH, NH_2, and NH groups, were visible in the IR spectrum (KBr/cm^{-1}) of compound **4a**.

A singlet signal at δ 5.92 ppm due to NH_2 protons, a singlet signal at δ 10.53 due to OH, and a singlet signal at δ 12.89 due to an NH proton were all visible in the ^1H NMR spectrum (ppm). Additionally, due to two aromatic protons, there were two doublets at δ 7.40 ($J = 9$ Hz), 7.78 ($J = 9$ Hz), a triplet, and a singlet signal at δ 7.55 and δ 7.96 ppm. The ^{13}C NMR spectra revealed three signals for 3C-pyrazole at δ 111.93, 150.31, and δ 158.69 ppm as well as a signal for CF_3 at δ 119.54 ppm in addition to the aromatic carbons. A molecular ion peak with the chemical
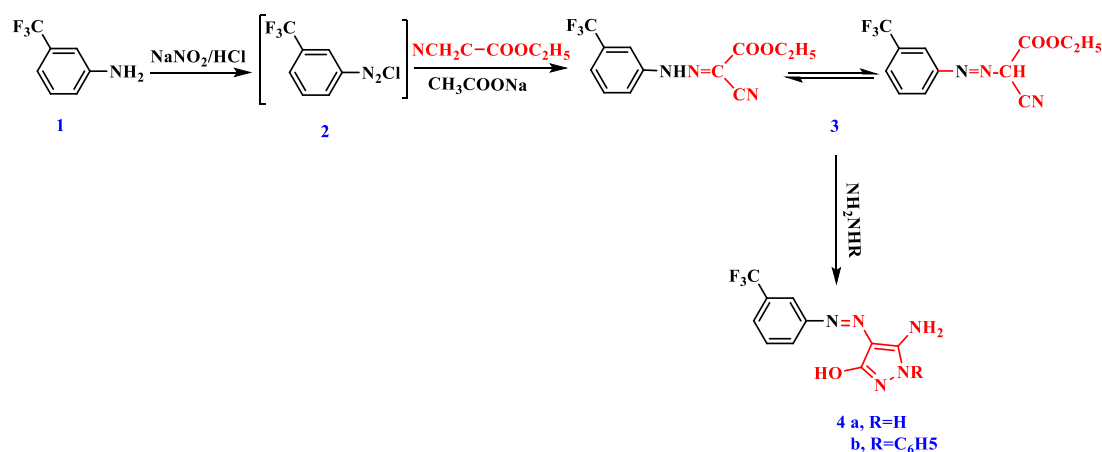
Scheme 1 Synthesis of 3-hydroxy pyrazole derivatives **4a&b**

Scheme 2 The use of 5-amino-4-(3-trifluoromethylphenyldiazenyl)-1H-pyrazol-3-ol (**4a**) to afford pyrazolo-pyrimidine derivatives **5-8**
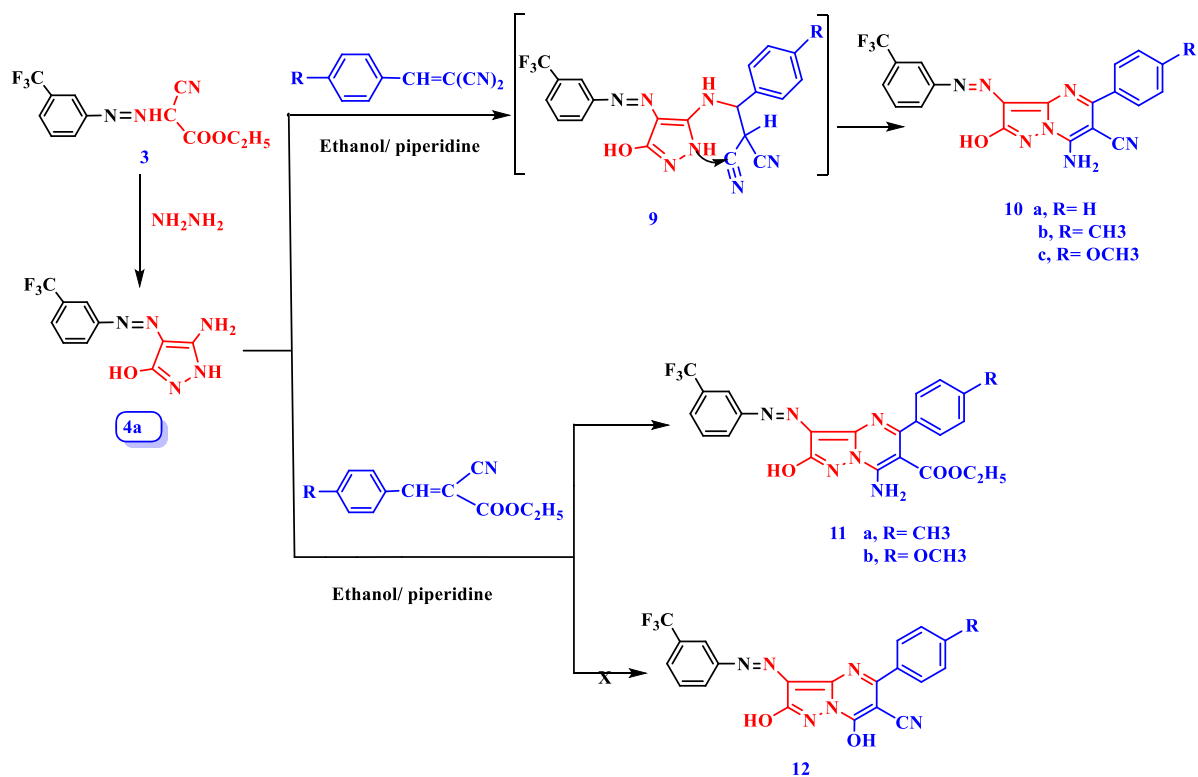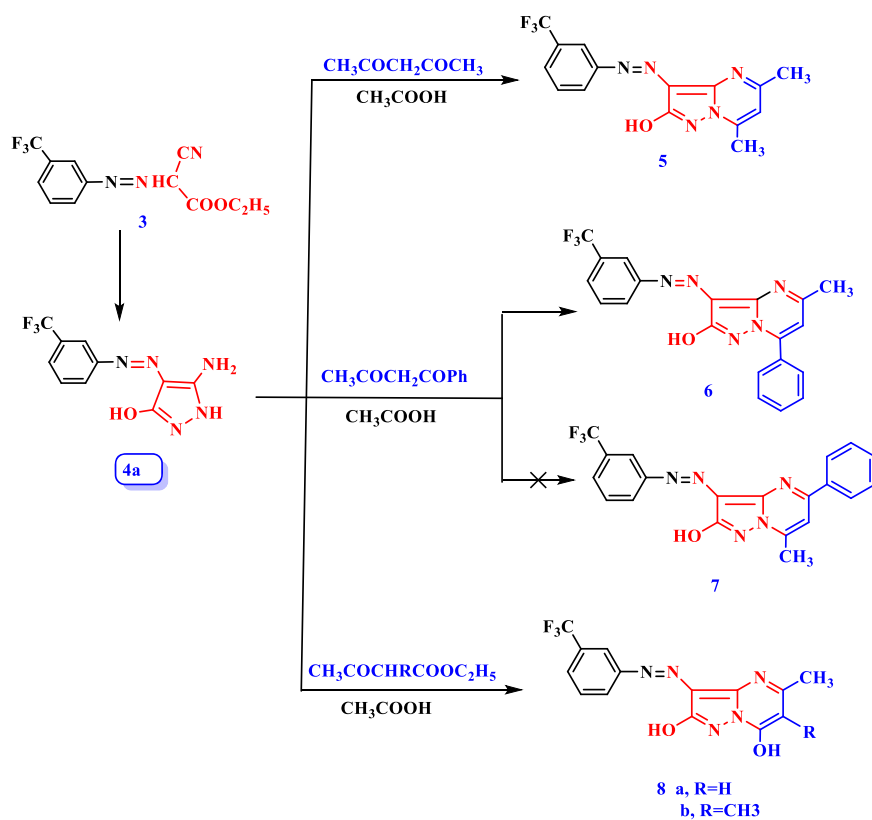
Scheme 3 Synthetic pathway of Pyrazolo-pyrimidine derivatives **10** & **11**
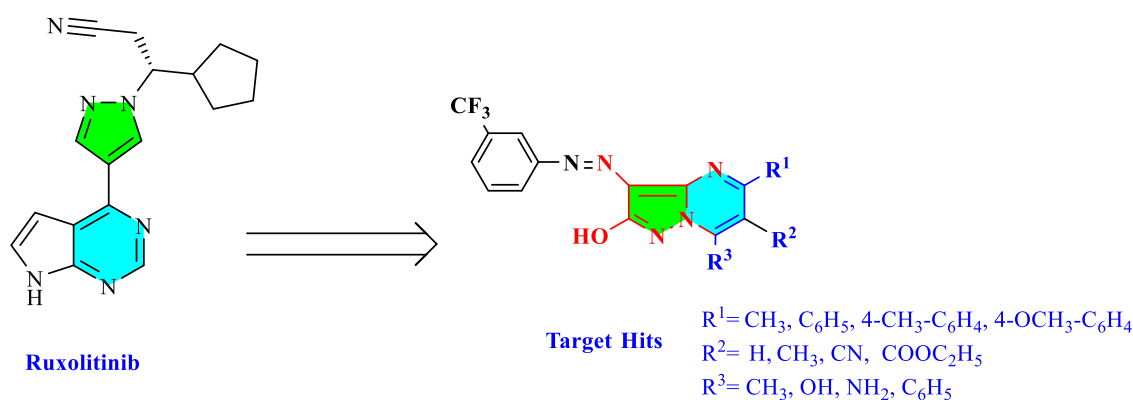
Fig. 1 Rational design of pyrazolo-pyrimidine molecules with different substitutions

formula $C_{10}H_8F_3N_5O$ was visible in the mass spectrum at $m/z = 271$ [M. +].

In continuation of this research interest in the synthesis of biologically important heterocyclic compounds, a series of new 2-hydroxypyrazolo[1,5-a]pyrimidines derivatives were synthesized starting with 5-amino-4-(3-trifluoromethylphenyldiazenyl)-1H-pyrazol-3-ol (**4a**). Thus, when reacting pyrazole derivative **4a** with acetylacetone in glacial acetic acid under reflux, 5,7-dimethylpyrazolo[1,5-a]pyrimidine (**5**) was afforded.

Based on analytical and spectral data, the structure of **5** was identified and validated (IR, MS, ^{1}H NMR, and ^{13}C NMR). Strong absorption bands at 3401 and 1635 cm^{-1}, which correspond to the OH and C=N groups, respectively, were visible in its IR spectra (KBr/cm^{-1}). Three singlets were visible in its ^{1}H NMR spectra, including CH-pyrimidine at δ 7.23 ppm and 2CH$_3$ protons at δ 2.56 and δ 2.60 ppm, respectively.

Additionally, two doublets of the aromatic protons were seen at δ 7.56 and δ 8.00 ppm, one triplet at δ 7.69 ppm, and one singlet at δ 8.05 ppm. Finally, a singlet was assigned at δ 7.01 ppm for the swapped D$_2$O proton from the OH proton. A molecular ion peak was visible in the mass spectrum at $m/z = 335$ (23.65%), which corresponds to the molecular formula $C_{15}H_{12}F_3N_5O$. A base peak was also visible at $m/z = 40$, which corresponds to $C_2O^{\neg \bullet+}$. Similar to this, when **4a** was combined with benzoyl acetone in acetic acid, the result was a substance that was constructed as either structure **6** or **7**. Using steric hindrance as justification, the structure of **7** was quickly abandoned. The use of spectrum data and elemental analysis supported the structure of **6**. A broad region of its IR spectra, corresponding to OH at 3460 cm^{-1} and C=N at 636 cm^{-1}, was visible. Three singlet signals, corresponding to CH$_3$, CH-pyrimidine, and OH, were detected in the sample's ^{1}H NMR spectra at δ 2.65, δ 7.44, and δ 8.08 ppm, respectively. A molecular ion peak at $m/z = 397$ [M.+, 23.65%] in the mass spectrum of compound **6** was seen together with a base

peak at $m/z = 131$. This peak corresponds to the molecular formula $C_{20}H_{14}F_3N_5O$.

Furthermore, it has been found that treatment of **4a** with ethyl acetoacetates in acetic acid led to the formation of a product that was formulated as pyrazolo[1,5-a]pyrimidines **8a&b** [62]. Compounds **8a&b** are assumed to be formed via initial condensation of the exocyclic amino function in **4a** with the carbonyl group in ethyl acetoacetate to give the intermediate which readily cyclized to the final isolable product. Structure **8** is suggested for the reaction product based on both elemental and spectral analyses. The IR spectrum of compound **8a** showed bands related to 2 OH and N=N functions which appeared at 3313, 3179, and 1566 cm^{-1} respectively, while compound **8b** appeared at 3176 cm^{-1} (OH). ^{1}H NMR spectrum for **8a** revealed two singlet signals at δ 2.37, 5.94 ppm assigned for CH$_3$ and CH-pyrimidine protons, the aromatic protons appeared as multiplet, doublet, and singlet signals at δ 7.38, 8.03, and 8.11 ppm respectively, while two exchangeable singlet signals appeared at δ 10.54, 12.85 ppm due to the two OH protons. ^{13}C NMR of compound **8a** showed methyl group at δ 19.00 besides the aromatic carbons. The mass spectrum of **8a** showed an ion peak at $m/z = 337$ corresponding to the molecular formula $C_{14}H_{10}F_3N_5O_2$ with a base peak at m/z 40 with $C_2H_2N^{\neg+}$ molecular formula.

Similar to the behavior of amino pyrazole [60] towards the activated double bonds, 2-hydroxy-5-amino pyrazole **4a** was reacted with arylidene-malononitriles in ethanol containing piperidine as a catalyst producing a product that was analyzed as 7-aminopyrazolo[1,5-a]pyrimidine **10a-c**. Structure **10** was established based on elemental analysis and spectral data. IR spectrum of **10b** showed bands related to NH$_2$, OH functions as two bands 3336 and 3125 cm^{-1}, and C≡N group at 2214 cm^{-1}. ^{1}H NMR spectrum of **10b** revealed a singlet signal at δ 2.39 ppm attributed to CH$_3$ and the NH$_2$ protons were observed at δ 5.95 ppm while a doublet signal appeared at δ 8.04 ppm and a singlet signal at δ 8.14 ppm beside the aromatic

protons were observed as multiplet in the region δ 7.33–7.96 ppm. ^{13}C NMR of **10b** showed signals at δ 21.46 ppm due to CH$_3$, δ 116.23 ppm (C≡N), δ 124.83 ppm (CF$_3$) besides the Ar-C. The mass spectrum of **10b** showed a molecular ion peak at $m/z = 437$ (21.96%) corresponding to a formula C$_{21}$H$_{14}$F$_3$N$_7$O.

The interaction of the amino pyrazole **4a** with the ethyl cyanocinnamates in ethanol that contains a little amount of piperidine, the 7-amino **11**, or the 7-hydroxy **12** appeared to provide probable products for such a reaction. On the other hand, spectral data allowed for the identification of the 7-aminoypyrazolo[1,5-*a*]pyrimidine **11** as the single reaction product. Compound **11** is thought to be created by first adding the exocyclic amino group from compound **4a** to the unsaturated system, cyclizing it by adding the pyrazole NH to the cyano group nucleophilically, and then spontaneously auto-oxidizing it by losing the H$_2$ molecule. Based on both elemental and spectral analyses, it was proposed that the reaction product has the structure of compound **11**. The IR spectrum of compound **11a** revealed the existence of absorption bands at 3427, 3308, and 1680 cm^{-1}, which correspond to the OH, NH$_2$, and C = O functions, respectively, however, the presence of the cyano group was absent. In its ^{1}H NMR spectra, CH$_3$ and CH$_2$-ester were seen as triplet and quartet at δ 0.89 and δ 4.0 ppm, respectively, and CH$_3$-phenyl was seen at δ 2.36 ppm.

Additionally, two singlet signals that represented the OH and NH$_2$ protons that were subsequently annihilated by D$_2$O occurred at δ 8.02 and δ 8.3 ppm.

Biological evaluation

In vitro cytotoxic activity

The newly synthesized hybrids, **4a**, **5**, **8a&b**, **10a-c**, **11a&b** were screened for their anticancer activity against three human cell lines which are liver carcinoma cell line (HepG-2), colon cancer cell line (HCT-116), and human breast cancer cell line (MCF-7) compared with the standard Imatinib as a reference drug.

It should be mentioned that (2,7-dihydroxy)pyrazolo-pyrimidine **8a,b** displayed potent anticancer activity compared to its mono-hydroxy analogs (**5**) were 2-3 fold decrease of activity upon replacement of the OH- position 7- with the CH$_3$. 5-Methyl-3-((3-(trifluoromethyl)-phenyl)diazenyl)pyrazolo[1,5-*a*]-pyrimidine-2,7-diol (**8a**) showed almost equipotent activity of imatinib against HepG-2, half potent of activity of imatinib against HCT-116 and 0.75 of activity of imatinib against MCF-7, and its analog **8b** showed twice the anticancer activity of imatinib against HepG-2, 1.25 of activity against MCF-7 and 1/6 of activity against HCT-116.

It is worth also mentioning that the 6-cyano-pyrazolopyrimidines **10b&c** bearing a substituted phenyl group at 5-position were by far much more effective anti-proliferative activity than their counterparts **10a** with a non-substituted phenyl analogous. Compound **10c** showed high potent anticancer activity five times of activity of the reference standard against HepG-2, almost half of the activity against HCT-116, and 0.75 of activity against MCF-7, at the same time compound **10b** exerted potent anticancer activity compared to the reference drug with (IC$_{50}$ = 7.9, 7.97, 10.1 µM/mL) respectively.

Except for compound **11b** against the HepG-2 cell line, it was found that replacement of the cyano group in position 6- of the pyrazolo-pyrimidine scaffold by acetate substituents as in compounds **11a** & **11b** lead to poor anticancer activity against all other tested cell lines.

Effect on normal cells The cytotoxic activities of the most promising compounds **8a**, **8b**, **10c**, and **11b** in normal non-cancer cells were examined for the selectivity of the pyrazolopyrimidine by cancer cells (WI-38 cells). As it appeared in Table 1, the most potent hybrids had IC$_{50}$ values ranging from 109.4 to 162.1 M. The selective index (SI) statistics in Table 1 show that the trifluoromethyl-phenyl core linked to pyrazolopyrimidine derivatives had a high degree of lethal selectivity. For example, the most potent hybrid, 7-amino-2-hydroxy-5-(4-methoxyphenyl)-3-((3-(trifluoromethyl)phenyl)diazenyl)pyrazolo[1,5-*a*]-pyrimidine-6-carbonitrile (**10c**), had

Table 1 In Vitro^a cytotoxic evaluation of the synthesized hybrids and Imatinib against three cell lines as well as normal cell

Cpd.	IC$_{50}$ µM/mL/SI^b			
	HepG-2	HCT-116	MCF-7	WI-38
4a	47.80 ± 3.79	43.60 ± 3.21	38.00 ± 2.65	ND
5	10.20 ± 0.90	14.80 ± 1.10	20.90 ± 1.62	ND
6	>50	>50	>50	ND
8a	6.07 ± 0.46 (24.32)	11.50 ± 0.94 (12.83)	9.98 ± 0.78 (14.79)	147.6 ± 2.78
8b	2.36 ± 0.14 (65.97)	4.13 ± 0.25 (37.70)	5.06 ± 0.36 (30.77)	155.7 ± 3.52
10a	>50	>50	>50	ND
10b	7.90 ± 0.44	7.97 ± 0.47	10.10 ± 0.92	ND
10c	1.14 ± 0.063 (142.19)	2.63 ± 0.16 (61.63)	3.53 ± 0.22 (45.92)	162.1 ± 3.75
11a	43.70 ± 3.23	>50	48.20 ± 3.87	ND
11b	5.25 ± 0.39 (20.84)	19.00 ± 1.60 (5.76)	22.90 ± 1.95 (4.78)	109.4 ± 2.1
Imatinib	5.50 ± 0.45	4.41 ± 0.33	6.06 ± 0.51	ND

^{a}Data represent the mean values of three independent determinations
^{b}SI Selectivity index = (IC$_{50}$ of WI-38)/(IC$_{50}$ of cancer cell line)
ND Not determined

the safest molecule with IC$_{50}$ (162.1 M) and the highest SI (142.19, 61.63, and 45.92). Simultaneously, dimethyl-3-((3-(trifluoromethyl)phenyl)diazenyl)pyrimidine-2,7-diol (**8b**) demonstrated IC$_{50}$ (89.75 M) with SI (65.97, 37.70, and 30.77) to the cell line examined.

SAR study In this work, compounds **4a**, **5**, **8a**&**b**, **10a-c**, **11a**&**b** were tested for their anticancer activity against three human cell lines: the HepG-2 liver carcinoma cell line, the HCT-116 colon cancer cell line, and the MCF-7 human breast cancer cell line.

From the structure of the newly synthesized hits, it was found that all compounds are similar in their structure to some extent as there is a substitution of trifluoromethyl (CF$_3$) on the phenyl ring as well as the presence of hydroxyl group on the pyrazole ring. The difference between the structures represented at the substitution on the pyrimidine ring.

Based on the screening results, it was discovered that (2,7-dihydroxy)pyrazolo-pyrimidine **8a,b** exhibited powerful anticancer activity in comparison to its mono-hydroxy analogues (**5**), with a 2-3 fold drop in activity upon substitution of the OH- position 7- with the CH$_3$ -pyrimidine-2,7-diol (**8a**) displayed almost equal imatinib activity against HepG-2, half-potent imatinib activity against HCT-116, and 0.75 imatinib activity against MCF-7, whereas **8b** displayed twice the imatinib anticancer activity against HepG-2, 1.25 imatinib activity against MCF-7, and 1/6 imatinib activity against HCT-116, this may be due to the presence of hydroxyl group on the pyrimidine ring which have positive mesomeric effect.

It's also important to note that the presence of substituted phenyl group at position 5 of the 6-cyano-pyrazolopyrimidines is important for the anticancer activity, compounds which have substituted phenyl groups at the 5-position, have far stronger antiprolifera-tive effects than their counterparts **10a**, which have non-substituted phenyl group. Furthermore, when the sub-stitution presented as methoxy group as in compound **10c** demonstrated extremely powerful anticancer activity, this may be due to the positive mesomeric effect of the methoxy group. Also, the presence of cyano group of such compounds **10b**&**c** found to have an effect on the anticancer activity because when it replaced by ester group as in compounds **11** the activity decreased against all tested cell lines.

Apoptosis detection studies

Effect on the active Caspase 3 level Caspase 3 activation is a hallmark of apoptosis and can be used in cell assays for the quantification of activators and death cascade inhibitors. The most active analogs of **8a**, **8b**, **10c**, and **11b** for their
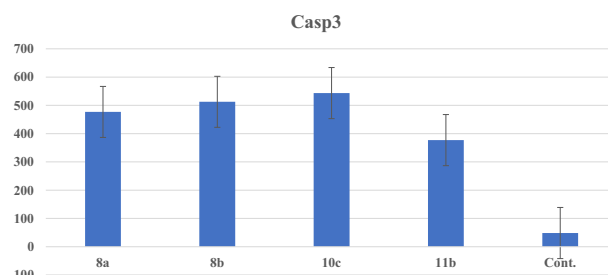

Fig. 2 The effect on apoptotic induction of Caspase-3 was shown by **8a**, **8b**, **10c**, and **11b**

Table 2 Effect on gene expression of some apoptosis key markers from compounds **8a**, **8b**, **10c**, and **11b**

Cpd. no.	Casp3 Pg/mL	Fold	BAX Pg/mL	Fold	Bcl-2 Pg/mL	Fold	BAX/Bcl-2 ratio
8a	476.840	9.86	378.50	9.62	1.470	3.708	35.69
8b	512.653	10.61	357.43	9.09	1.974	2.76	25.10
10c	543.523	11.24	381.62	9.70	1.209	4.51	43.75
11b	377.096	7.81	327.80	8.33	2.081	2.62	21.83
Cont.	48.340	1	39.33	1	5.451	1	1

impact on Caspase 3 were assessed. Compounds **8b** and **10c** have increased their active level of Caspase 3 to 10.61, and 11.24 folds, respectively, about the control while **8a** and **11b** increased their active level of Caspase 3 by 9.86, and 7.81 folds, respectively, which is considered an Apoptosis Marker (Fig. 2 & Table 2).

Effect on mitochondrial apoptosis pathway proteins BAX and Bcl-2 Various direct activators for BAX (pro-apopto-tic) were found to promise cancer therapy with the benefits of specificities and the potential to overcome chemical and radial resistance. If BAX values in mitochondria are to be increased, levels of Bcl-2 (anti-apoptotic) in the mitochon-drial membrane may have to be reduced. For their effect on some key apoptosis markers, BAX and Bcl-2 the most active **8a**, **8b**, **10c**, and **11b** were assessed on human liver adenocarcinoma epithelial cells (HepG-2 cells) Table 2.

Results found that the pro-apoptotic protein BAX was increased by all tested compounds and the anti-apoptotic protein Bcl-2 was reduced (Table 2). Compound **10c** produced the best results, increasing the level of BAX by 11.24 folds while decreasing the level of Bcl-2 by 4.51 folds when compared to the control. Compounds **8a**, **8b**, **10c**, and **11b** on the other hand, increased BAX levels by 7.81–10.61folds while decreasing Bcl-2 levels by 2.62–3.708 folds.

The ratio of the two proteins is a much more important parameter. Thus, the BAX/Bcl-2 ratio for compound **10c** was calculated to be 43.75 folds higher than the control,

while the other tested compounds were found to be 21.83–35.69 folds higher, indicating that these compounds shifted the cells toward apoptosis.

Cell cycle analysis

The most promising two derivatives **8b**, and **10c** were selected and studied for cell cycle progression and apoptosis percentage produced by pyrazolo-pyrimidine derivatives based on the antiproliferative activity, BAX, and Bcl-2 gene expression obtained earlier. On HepG-2 cancer cells, cell cycle arrest was performed, and the results are shown in Table 3 and Figs. 3 and 4.

The investigated drugs caused PreG1 apoptosis and cell growth arrest in HepG-2 at the G2/M phase, as illustrated in Fig. 3 and Table 3. Dimethyl-3-((3-(trifluoromethyl)phenyl) diazenyl)7-amino-2-hydroxy-5-pyrimidine-2,7-diol (**8b**) and pyrimidine-2,7-diol(4-methoxyphenyl)-3-((3-(trifluoromethyl) phenyl)-diazenyl)pyrazolo[1,5-a]pyrimidine-6-carbonitrile (**10c**) causes HepG-2 cells to aggregate by 39.58 and 41.29 percent at the G0-G1 stages, respectively, as well as a 26.29 and 26.64 percent rise in the G2/M phase percentage, compared to 17.68 percent in untreated cells.

Fused pyrazolo-pyrimidine hybrids **8b** and **10c** cause apoptosis and halt the cell cycle by approximately 73.36 and 73.71 percent, respectively, in the Pre-G1 and G2-M stages. Finally, our proposed derivatives with various substituents **8b**, and **10c** can be employed as inhibitors and trigger apoptosis in various stages.

Table 3 Effect of compounds **8b** and **10c** on the cell cycle of HepG-2 cell line

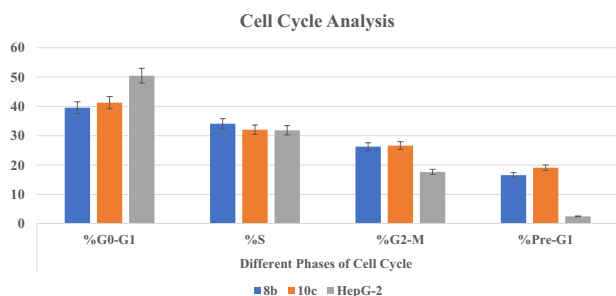| Cpd. no.	Results			
	%G0-G1	%S	%G2-M	%Pre-G1
8b	39.58	34.13	26.29	16.59
10c	41.29	32.07	26.64	19.11
HepG-2	50.46	31.86	17.68	2.55

Fig. 3 On the HepG-2 cell line, cell cycle analysis and apoptotic effect of **8b** and **10c**

Annexin V-FITC apoptosis assay

Using the follow cytometry approach, double labeling Annexin V/propidium iodide was utilized to identify the mechanism of cell death and apoptosis-inducing effects [19]. Apoptosis is a regular and active process, whereas necrosis is an accidental and passive cell death. The data obtained after the pyrazolo-pyrimidine derivatives **8b** and **10c** were treated with 5 μM and incubated on HepG-2 cells for 24 h are displayed in Table 4 and Fig. 5.

We detected an increase in the total percentage of apoptosis because the tested derivatives that exhibit total apoptosis ranged from 16.59% to 19.11% compared to 2.55% for standard HepG-2 cells. Moreover, the percentage in the early stage varies from 5.13, and 2.61% for **8b**, and **10c** respectively.

Finally, it can conclude that the effect of the most promising derivatives **8b**, and **10c** when treated with HepG-2 leads to an increase in the sensitivity to apoptosis by different percentages in different stages and therefore increase in total apoptosis percentage and these data support the higher values on antiproliferative against HepG-2 (< 5 μM).

EGFR inhibition assay

Because it is critical for several biological processes and malignancies genesis and progression, such as cell proliferation, adhesion, migration, differentiation, and survival, the epidermal growth factor receptor (EGFR) is an appealing and clinically-validated therapeutic target in cancer therapy. EGFR can lead to dysregulation by two different mechanisms, one of which is high EGFR expression, leading to increased output for receiver signaling whereas the second mechanism involves ligand over-expression and increases EGFR signaling activity despite normal or low levels of receptor expression [63, 64]. In this study, we chose the most promising compounds **8b** and **10c** for EGFR enzymatic activity assays employing HepG-2 cancer cells to elucidate the mechanism of these potent compounds based on the results of the antiproliferative activity.

Results of the wide type EGFR^{WT} on cancer cells HepG-2 were shown in Table 5 to be half the maximum IC$_{50}$ (nM) inhibitory concentration. Pyrimidine-2,7-diol(4-methoxyphenyl)-3-((3-(trifluoromethyl)phenyl)diazenyl)pyrazolo[1,5-a]6-carbonitrile-pyrimidine (**10c**), the most powerful derivatives were displayed with IC$_{50}$ equal 0.079 nM. Compound **8b**, on the other hand, reduced the enzymatic activity of EGFR^{WT} with an IC$_{50}$ value of 0.098 nM.

Because of the significance of EGFR, which can also be identified by transducing the mitogenic signals as members of the membrane-bound receptor tyrosine kinase family [54]. To evaluate the activity and selectivity of new compounds, we selected the most promising compounds for the additional in vitro EGFR $^{L858R-TK}$ that is expressed as IC$_{50}$
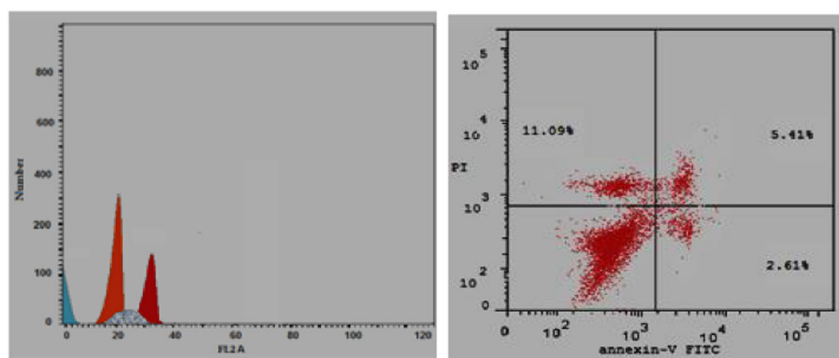
Fig. 4 Cell cycle analysis (**A**) Control HepG-2, (**B**) for compound **8b**, (**C**) for compound **10c**, by flow cytometry using the PI staining method
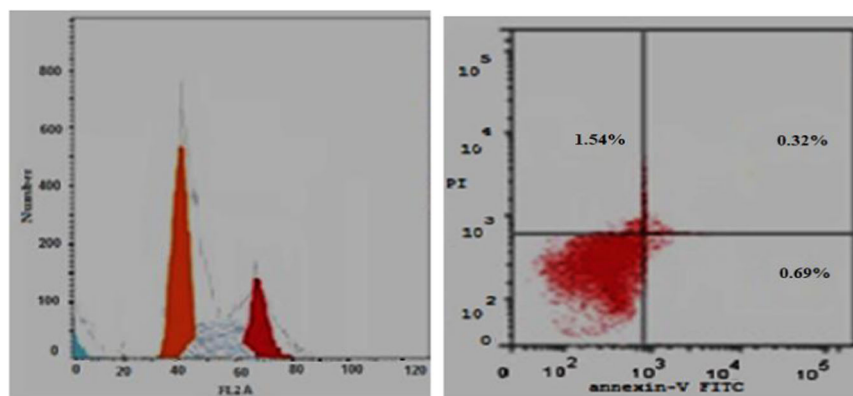
A (HepG-2)
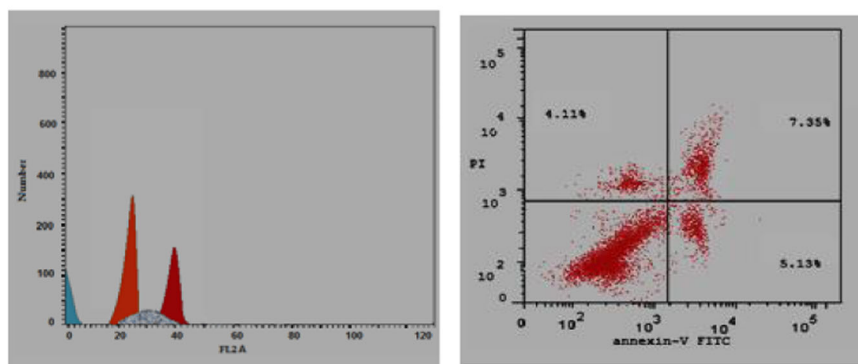
B (8b/HepG-2)

C (10c/HepG-2)

(nM). In comparison with the positive control of lapatinib (IC$_{50}$ = 38.60), compound **10c** was the most potent inhibitory activity for EGFR $^{L858R-TK}$ in IC$_{50}$ (36.79 nM). Derivatives **8b** revealed the least IC$_{50}$ = 40.157 nM with an inhibitor EGFR $^{L858R-TK}$ of lower activity than the positive control towards EGFR^{WT}.

Our research was expanded to include the most promising two derivatives **8b**, and **10c** against the further kinase EGFR$^{L858R/T790M}$ double mutant with Lapatinib and Erlotinib as reference drugs, and they inhibited the enzymatic activity against EGFR$^{L858R/T790M}$ double mutant with IC$_{50}$ values ranging from (0.299–0.301 nM) compared to Lapatinib and Erlotinib (0.188 and 0.209 nM) correspondingly.

In silico computational studies

In-silico ADME properties studies Along with all the synthesized compounds, the standard reference medication,

Table 4 Percentage of cell death after treatment with most promising compounds **8b**, and **10c**

Cpd. No.	Apoptosis			Necrosis
	Total	Early	Late	
8b	16.59	5.13	7.35	4.11
10c	19.11	2.61	5.41	11.09
HepG-2	2.55	0.69	0.32	1.54
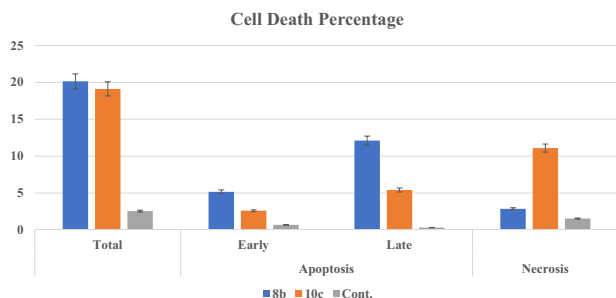
Fig. 5 The percentage of cell death caused by compounds **8b** and **10c** on HepG-2 cells is depicted in a schematic diagram

Table 5 IC$_{50}$ of the representative anticancer active compounds on different EGFR kinases assay

Cpd. No.	Enzyme inhibitory activity IC$_{50}$ [a]		
	EGFR^{WT} (nM)	EGFR $^{L858R\text{-}TK}$ (nM)	EGFR L/T[b]
8b	0.098	40.157	0.301
10c	0.079	36.79	0.299
Erlotinib	0.0630	59.61	0.209
Lapatinib	0.0339	38.60	0.188

[a]data are an average of three independent results

[b]EGFR L/T = double mutant EGFR L858R/T790M, (-) means not determined

Imatinib, was submitted in silico physicochemical, pharmacokinetic/ADME, and drug-likeliness properties. Physicochemical metrics such as molar refractivity, atomic class count, and the number of rotatable connections, as well as lipophilicity and water solubility, have been reported. The TPSA is a good physiochemical vector for regulating drug transportation properties (Topological Polar Surface Area). The reporting equation (ABS = 109-(0.345 X TPSA) was used to try to predict the absorption rate of all test compounds [65].

As shown Table 6 lists these physicochemical features. The absorption rate varies between 61.84 percent and 83.08 percent among the compounds chosen. With a median of 74.62 percent and 83.08 percent of reference and manufactured pharmaceuticals, respectively, some compounds in water with a good molar refractiveness are moderately soluble and moderate to goodly absorbent.

Table 7 lists the pharmacokinetic and ADME properties of the compounds studied. Compounds **4a**, **5**, **8a**, and **8b** as well as Imatinib have demonstrated that they are easily absorbed by the gastrointestinal (GI) system and all compounds except Imatinib are not P-gp inhibitors (p-glycoprotein).

All of the chemicals examined, as well as Imatinib, were unable to pass the blood-brain barrier (BBB), so they have no CNS side effects. Furthermore, all of the Cytochrome P450 isomers examined are inhibited by Imatinib except CYP1A2. Many of the chemicals being studied block one of the other Cytochrome P450 isomers. The coefficient values for skin permeability (log Kp; with Kp in cm/s) of the evaluated substances were found to be minimal (Table 7).

Lipinski [62], Ghose [63], Veber [64], Egan [65], and Muegge [66] had to assess the molecule as a potential drug candidate due to the several regulations governing drug-likeness. Table 8 shows the number of infractions of the previously named regulations, as well as their bioavailability scores. The Lipinski (Pfizer) strain is the fashion setter for the rule-of-five (RO5) legislation, which states that all substances examined are identical to pharmaceuticals. According to the Ghose and Muegge law, all compounds follow the rule and are medication candidates, according to the forecasts. During the assessment process utilizing the Veber and Egan guidelines, most of the tested hybrids showed drug-like properties. All of the compounds studied had a bioavailability value of 0.55.

Molecular docking study The ATP binding pocket of EGFR PDB (1M17) [24] was used to simulate molecular docking to explore various binding conformations and get deeper insights into the structure-activity relationship as well as comprehend the potency of the newly developed Pyrazolopyrimidine derivatives **8b**, **10c**. The co-crystalized ligand 4-anilinoquinazoline inhibitor (**Erlotinib**) was found to be deeply bounded inside the active site of the pocket through a self-docking process with a small RMSD = 1.41 and binding energy −10.622 Kcal/mol, through one hydrogen bond acceptor with **Met769** with the nitrogen of quinazoline with bond length 3.24 °A, and two arene-H (PI-H) bonds of phenyl and pyrimidine ring with **Leu694** with bond length 4.07 and 4.21 respectively (Fig. 6).

Furthermore, **Lapatinib** as a co-crystallized ligand was re-docked into the active site of EGFR PDB (1M17) to validate the docking protocol giving an energy score of −9.685 kcal/mol with a root mean square deviation (RMDS) value equal to 2.02 Å (Fig. 7).

Then, the newly synthesized compounds **8b**, and **10c** were docked into the ATP-active site of EGFR and the results were depicted in Figs. 8, 9 with energy scores of −10.606, and −10.405 kcal/mol, respectively.

Table 6 Physicochemical properties of the newly synthesized compounds

Cpd. No.	Fraction Csp3[a]	No. of rotatable bonds	HBA[b]	HBD[c]	iLogP[d]	Molar Refractivity	Log S[e]	TPSA[f]	In silico % absorption
4a	0.10	3	7	3	1.46	60.64	S	99.65	74.62
5	0.20	3	8	1	2.98	80.56	MS	75.14	83.08
6	0.10	4	8	1	3.77	101.03	PS	75.14	83.08
8a	0.14	3	9	2	2.58	77.62	MS	95.37	76.10
8b	0.20	3	9	2	2.82	82.59	MS	95.37	76.10
10a	0.05	4	9	2	2.63	105.19	PS	124.95	65.89
10b	0.10	4	9	2	3.03	110.15	PS	124.95	65.89
10c	0.10	5	10	2	2.90	111.68	PS	134.18	62.71
11a	0.17	7	10	2	3.75	121.52	PS	127.46	65.03
11b	0.17	8	11	2	3.26	123.05	PS	136.69	61.84
Imatinib	0.24	8	6	2	4.04	154.50	PS	86.28	79.23
Erlotinib	0.27	10	6	1	3.67	111.40	PS	74.73	83.21815
Lapatinib	0.17	11	8	2	4.20	153.88	IS	114.73	69.41815

[a]The ratio of sp^3 hybridized carbons over the total carbon count of the molecule; [b]number of hydrogen bond acceptors; [c]number of hydrogen bond donors; [d]lipophilicity; [e]Water solubility (SILICOS-IT [PS = Poorly soluble, MS = Moderately Soluble, S = Soluble]); [f]topological polar surface area (Å^2)

Table 7 Pharmacokinetic/ADME properties of the tested novel compounds

Cpd. No.	Pharmacokinetic/ADME properties								
	GI abs[a]	BBB permeant[b]	P-gp substrate[c]	CYP1A2 inhibitor[d]	CYP2C19 inhibitor[e]	CYP2C9 inhibitor[f]	CYP2D6 inhibitor[g]	CYP3A4 inhibitor[h]	Log K_p[i] (cm/s)
4a	High	No	No	No	No	No	No	No	−6.17
5	High	No	No	Yes	No	Yes	No	No	−5.67
6	Low	No	No	Yes	No	Yes	No	No	−5.15
8a	High	No	No	Yes	No	No	No	No	−5.99
8b	High	No	No	Yes	No	No	No	No	−5.81
10a	Low	No	No	Yes	No	Yes	No	No	−5.65
10b	Low	No	No	Yes	No	Yes	No	No	−5.48
10c	Low	No	No	Yes	No	Yes	No	No	−5.86
11a	Low	No	No	Yes	Yes	Yes	No	No	−5.41
11b	Low	No	No	Yes	Yes	Yes	No	No	−5.79
Imatinib	High	No	Yes	No	Yes	Yes	Yes	Yes	−6.81
Erlotinib	High	Yes	No	Yes	Yes	Yes	Yes	Yes	−6.35
Lapatinib	Low	No	No	No	Yes	Yes	Yes	Yes	−6.21

[a]Gastro Intestinal absorption, [b]Blood Brain Barrier permeant, [c]P-glycoprotein substrate, [d]CYP1A2: Cytochrome P450 family 1 subfamily A member 2 (PDB:2HI4), [e]CYP2C19: Cytochrome P450 family 2 subfamily C member 19 (PDB:4GQS), [f]CYP2C9: Cytochrome P450 family 2 subfamily C member 9 (PDB:1OG2), [g]CYP2D6: Cytochrome P450 family 2 subfamily D member 6 (PDB:5TFT), [h]CYP3A4: Cytochrome P450 family 3 subfamily A member 4 (PDB:4K9T), [i]Skin permeation in cm/s

As shown in Fig. 8, dimethyl-3-((3-(trifluoromethyl) phenyl)diazenyl)pyrazolo[1,5-*a*]pyrimidine-2,7-diol **(8b)** formed a hydrogen bond donor between the oxygen of the hydroxyl group at the pyrazole ring and the backbone of **Met769** (distance: 2.95 Å). Moreover, the trifluoromethyl group shared fixation through the H-bonds acceptor between the fluoride atom and the side chain of **Lys692** through bond length (3.37 °A). Additionally, the five-membered pyrazole

scaffold improved fixation within the active site of EGFR through arene-hydrogen interaction with the key amino acid **Leu694** (distance: 4.00 °A).

The adjacent amino and cyano fragments play an essential role in the fixation of 7-Amino-2-hydroxy-5-(4-methoxyphenyl)-3-((3-(trifluoromethyl)phenyl)diazenyl)pyrazolo[1,5-*a*] pyrimidine-6-carbonitrile **(10c)** within EGFR through the formation of two H-bonding with the backbone of **Met769**;

Table 8 Drug likeness predictions and bioavailability scores of **4a-11b** as well as Imatinib

| Cpd. No.	Lipinski (violations)	Ghose (violations)	Veber (violations)	Egan (violations)	Muegge (violations)	Bioavailability Score	PAINS Alerts	Synthetic accessibility
4a	Yes	Yes	Yes	Yes	Yes	0.55	1	2.73
5	Yes	No (1)	Yes	Yes	Yes	0.55	1	3.08
6	Yes	No (1)	Yes	No (1)	No (1)	0.55	1	3.38
8a	Yes	Yes	Yes	Yes	Yes	0.55	1	3.07
8b	Yes	Yes	Yes	Yes	Yes	0.55	1	3.19
10a	Yes	No (1)	Yes	No (1)	Yes	0.55	1	3.47
10b	Yes	No (1)	Yes	No (1)	Yes	0.55	1	3.59
10c	Yes	No (1)	Yes	No (1)	Yes	0.55	1	3.57
11a	Yes	No (2)	Yes	No (1)	No (1)	0.55	1	3.83
11b	Yes	No (2)	Yes	No (2)	No (2)	0.55	1	3.82
Imatinib	Yes	No (2)	Yes	Yes	Yes	0.55	0	3.78
Erlotinib	Yes	Yes	Yes	Yes	Yes	0.55	0	3.19
Lapatinib	Yes	No (3)	No (1)	No (1)	No (1)	0.55	0	4.05

Fig. 6 2D & 3D interaction maps of Erlotinib inside the 1M17 active site
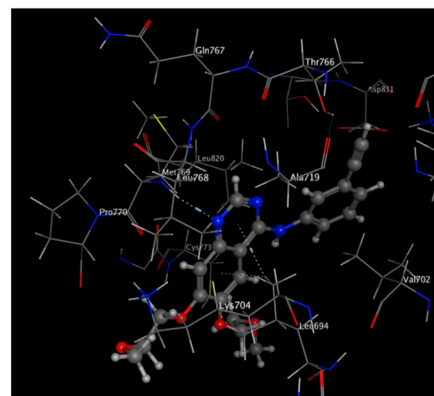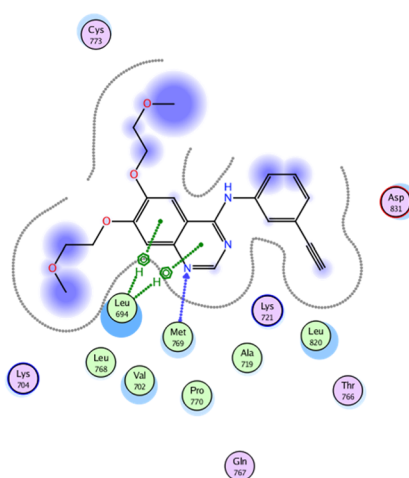
Fig. 7 2D & 3D interaction maps of **Lapatinib** inside the 1M17 active site
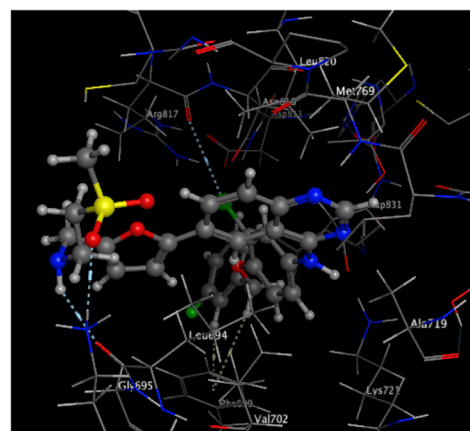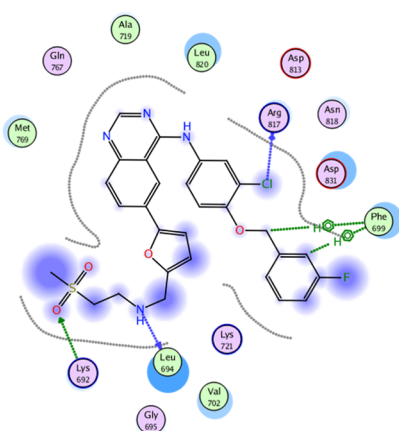
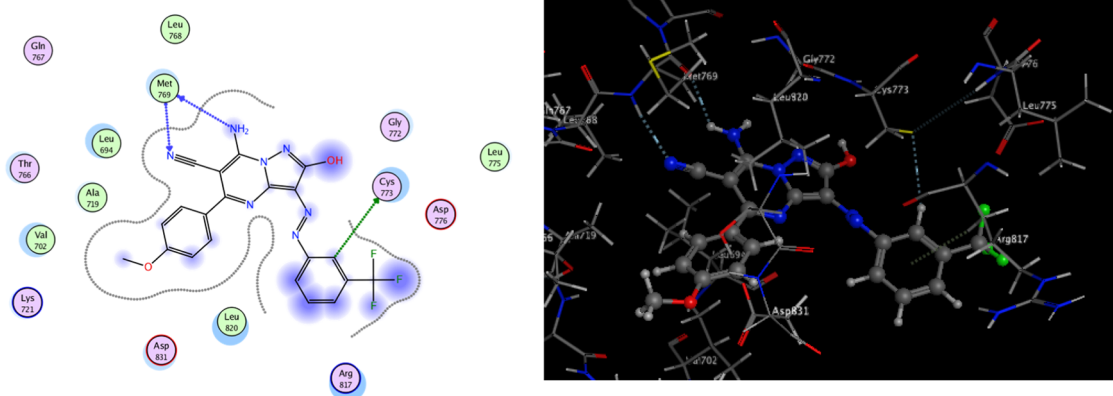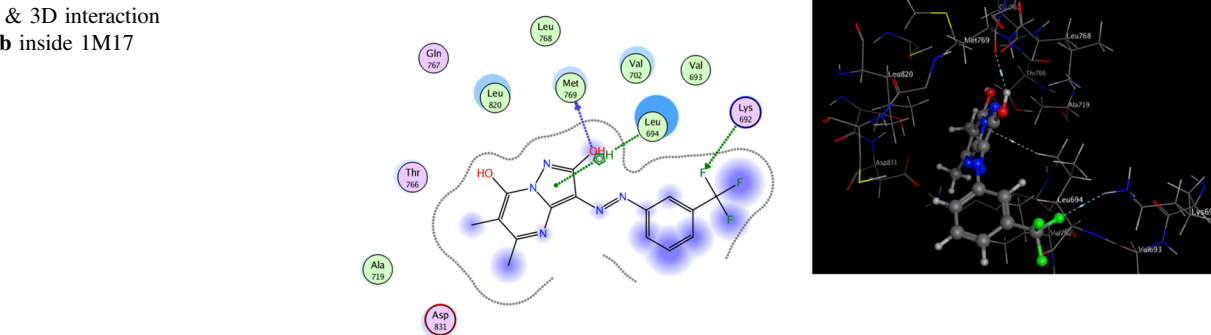**Fig. 8** 2D & 3D interaction maps of **8b** inside 1M17 active site

Fig. 9 2D & 3D interaction maps of **10c** inside 1M17 active site

one is donor with the proton of NH_2 group and the other is acceptor with the nitrogen of cyano group (distance: 3.09 and 3.19 Å, respectively). Moreover, the trifluoromethyl-phenyl assisted the binding via hydrogen bond donor between the carbon 2 of the phenyl ring with the sidechain of **Cys773** (distance: 4.14 Å) (Fig. 9).

Conclusion

The anticancer activity of a group of pyrazolo[1,5-*a*]pyrimidine derivatives **5–11** against the HepG-2, HCT-116, and MCF-7 cell lines was investigated. On liver cancer cells, the new hits had a stronger cytotoxic effect. Two compounds stood out as the most promising among the four effective derivatives (**8a**, **8b**, **10c**, and **11b**), with IC_{50} values that are greater than those of imatinib (2.360.14 and 1.140.063 μM, respectively). These compounds were subjected to further investigation for their apoptotic effect as Caspase 3, BAX, and Bcl-2. The two most promising drugs, **8a** and **10c**, produced cell cycle arrest at the apoptotic-specific Pre-G1 and G2/M stages, respectively. With Lapatinib and Erlotinib serving as standards, the greatest activity compounds, **8a** and **10c**, were tested against the in vitro EGFR L858R-TK and EGFRL858R/T790M double

mutant. ADMET as well as docking studies were performed with good results. For a deeper knowledge of the anticancer activity, research into pyrazoles and pyrazolopyrimidine rings containing azo and trifluoromethyl moieties would be extremely valuable.

Experimental sections

Chemistry

The melting points for the newly synthesized compounds were recorded using the LA 9000 SERIS Electrothermal Digital Melting Point Apparatus and were not adjusted. On a Nikolet IR 200 FT IR Spectrophotometer at the Pharmaceutical Analytical Unit, Faculty of Pharmacy, Al-Azhar University, and a Cary IR 630 FT IR Spectrophotometer at the Analytical Unit, Faculty of Science (boys), Al-Azhar University, IR Spectra were determined using the KBr disc technique. A Gemini Mercury 400 and 100 MHz NMR Spectrometer was used to determine the ^{1}H and ^{13}C NMR spectra at the Ministry of Defense's Chemical Warfare Department's Main Chemical Warfare Laboratories. Chemical shifts were evaluated in ppm relative to TMS as an internal standard (= 0 ppm), coupling constant *J* in Hz, and

solvents were DMSO-d_6 and CDCl$_3$. At Al-Azhar University's Regional Center for Mycology and Biotechnology, mass spectra were acquired at 70 eV using a Schimadzu GC/ MS-QP5050A Spectrometer with the DI-50 unit. Al-Azhar University's Regional Center for Mycology and Biotechnology conducted the microanalysis. Anticancer activity was tested in a local strain identified in the Regional Center for Genetic Engineering at Al-Azhar University's Faculty of Science (Boys), with findings within ±0.4 percent of the calculated value. Apoptosis markers, and EGFR, both wide and mutant, were carried out in VACSERA, Cairo, Egypt.

Ethyl 2-cyano-2-(2-(3-trifluoromethyl)phenylhydrazono) acetate (3)

To an ice-cooled solution of *m*-trifluoromethylaniline **1** (1.61 g, 0.01 mol) in hydrochloric acid (2.5 mL) and distilled water (5 mL), a solution of sodium nitrite (0.69 g, 0.013 mol) in distilled water (5 mL) was added. The cold diazotized solution was then added portion-wise to a well-stirred cold solution of ethyl cyanoacetate (1.13 mL, 0.01 mol), in 50% aqueous ethanol (10 mL) containing sodium acetate (0.9 g, 0.01 mol). The reaction mixture was kept on ice for 8 h. and then filtered and the obtained solid was dried and crystallized from ethanol.

Yield: 78% as yellow crystals; m.p.: 119-121 °C; IR: ν/cm^{-1}: 3218 (NH), 3081 (CH-aromatic), 2986 (CH-aliphatic), 2219 (C≡N), 1741 (C=O), 1603 (C=N), 1564 (N=N); ^{1}H NMR (400 MHz, DMSO-d_6) δ/ppm: 1.26 (t, 3H, CH$_2$CH$_3$), 4.26 (q, 2H, CH$_2$CH$_3$), 7.47 (d, 1H, $J = 9$ Hz, Ar-H), 7.61 (t, 1H, Ar-H), 7.71 (d, 1H, $J = 9$ Hz, Ar-H), 7.76 (s, 1H, Ar-H), 12.38 (s,1H, NH exchangeable by D$_2$O).

5-Amino-4-((3-(trifluoromethyl)phenyl)diazenyl)-1*H*-pyrazol-3-ol (4a) and 5-amino-1-phenyl-4-((3-(trifluoromethyl)phenyl)diazenyl)-1*H*-pyrazol-3-ol (4b)

A solution of **3** (2.85 g, 0.01 mol) and hydrazine hydrate or phenyl hydrazine (0.01 mol) in ethanol (30 mL) was heated under reflux for 8–12 h. The reaction mixture was cooled and the solid product was collected and recrystallized from ethanol.

5-Amino-4-((3-(trifluoromethyl)phenyl)diazenyl)-1*H*-pyrazol-3-ol (4a)

Yield 79% as bronze needles; m.p.: 211–213 °C; IR: ν/cm^{-1}: 3403, 3326, 3128 (OH & NH$_2$ & NH), 3040 (CH-aromatic), 1568 (N=N); ^{1}H NMR (300 MHz, DMSO-d_6) δ/ppm: 5.92 (s, 2H, NH$_2$ exchangeable by D$_2$O), 7.40 (d, 1H, $J = 7.5$ Hz, Ar-H), 7.55 (t, 1H, $J = 7.95$ Hz, Ar-H), 7.78 (d, 1H, $J = 8.1$ Hz, Ar-H), 7.96 (s, 1H, Ar-H), 10.53 (s, 1H,

OH exchangeable by D$_2$O), 12.89 (s, 1H, NH exchangeable by D$_2$O); ^{13}C NMR (100 MHz, CDCl$_3$) δ: 111.93, 150.31, 158.69 (3C-pyrazole), 119.54 (CF$_3$), 120.39, 123.13, 125.40, 128.56, 130.20, 143.43 (Ar-C); MS (*m/z*): 271 (M$^{.+}$, 65.55%), 145 (40.57%), 126 (100.0%); Anal.Calcd for C$_{10}$H$_8$F$_3$N$_5$O (271.20): C, 44.29; H, 2.97; N, 25.82; Found: C, 44.37; H, 2.98; N, 26.07%.

5-Amino-1-phenyl-4-((3-(trifluoromethyl)phenyl)diazenyl)-1*H*-pyrazol-3-ol (4b)

Yield 75% as black crystals; m.p.: 192-194 °C; IR: ν/cm^{-1}: 3431, 3298, 3173 (OH & NH$_2$), 3060 (CH-aromatic), 1568 (N=N); ^{1}H NMR (300 MHz, DMSO-d_6) δ/ppm: 6.55 (s, 2H, NH$_2$ exchangeable by D$_2$O), 7.13 (d, 1H, $J = 6.9$ Hz, Ar-H), 7.38 (t, 1H, $J = 8.1$ Hz, Ar-H), 7.43 (d, 1H, $J = 4.5$ Hz, Ar-H), 7.45 (t, 1H, $J = 7.5$ Hz, Ar-H), 7.59 (t, 1H, $J = 8.1$ Hz, Ar-H), 7.61 (d, 2H, $J = 8.1$ Hz, Ar-H), 7.90 (d, 2H, $J = 8.7$ Hz, Ar-H), 12.92 (s, 1H, OH exchangeable by D$_2$O); MS (*m/z*): 347 (M$^{.+}$, 81.83%), 77 (100.0%); Anal.Calcd for C$_{16}$H$_{12}$F$_3$N$_5$O (347.29): C, 55.33; H, 3.48; N, 20.17; Found: C, 55.49; H, 3.56; N, 20.44%.

5,7-Dimethyl-3-((3-(trifluoromethyl)phenyl)diazenyl) pyrazolo[1,5-*a*]pyrimidin-2-ol (5)

Acetylacetone (1.00 mL, 0.01 mol) was added to a solution of **4a** (2.71 g, 0.01 mol) in acetic acid (20 mL). The reaction mixture was heated under reflux for 6 h. The reaction mixture was cooled and the solid product was collected and crystallized from benzene.

Yield 77% as orange crystals; m.p.: 209-211 °C; IR: ν/cm^{-1}: 3401 (OH), 3056 (CH-aromatic), 2850 (CH-aliphatic), 1635 (C=N), 1551 (N=N); ^{1}H NMR (400 MHz, DMSO-d_6) δ/ppm: 2.56, 2.60 (2 s, 6H, 2CH$_3$), 7.23 (s, 1H, CH-pyrim.), 7.01 (s, 1H, OH; exchangeable by D$_2$O), 7.65 (d, 1H, $J = 8$ Hz, Ar-H), 7.69 (t, 1H, $J = 8$ Hz, Ar-H), 8.00 (d, 1H, $J = 8$ Hz, Ar-H), 8.05 (s, 1H, Ar-H); ^{13}C NMR (100 MHz, DMSO-d_6) δ 17.05, 24.47 (2CH$_3$), 116.09 (CF$_3$), 56.47, 147.46, 149.54 (3C-pyrazole), 114.11, 145.12, 162.67 (3C-pyrimidine), 123.12, 124.26, 125.83, 130.44, 130.76, 131.12 (Ar-C); MS (*m/z*): 335 (M$^{.+}$, 23.65%), 190 (91.58%), 162 (59.16%), 40 (100.0%); Anal.Calcd for C$_{15}$H$_{12}$F$_3$N$_5$O (335.28): C, 53.73; H, 3.61; N, 20.89; Found: C, 54.01; H, 3.66; N, 21.13%.

5-Methyl-7-phenyl-3-((3-(trifluoromethyl)phenyl)diazenyl) pyrazolo[1,5-*a*]pyrimidin-2-ol (6)

Benzoyl acetone (1.62 mL, 0.01 mol) was added to a solution of **4a** (2.71 g, 0.01 mol) in acetic acid (20 mL).

The reaction mixture was heated under reflux for 6 h. The reaction mixture was cooled and the solid product was collected and crystallized from Ethanol/benzene mixture.

Yield: 79% as orange crystals; m.p.: 257-259 °C; IR: ν/cm^{-1}: 3460 (br OH), 3060 (CH-aromatic), 2850 (CH-aliphatic), 1636 (C=N), 1536 (N=N), ^{1}H NMR (400 MHz, DMSO-d_6) δ/ppm: 2.65 (s, 3H, CH$_3$), 7.44 (s, 1H, CH-pyrim.), 7.60-7.73 (m, 7H, Ar-H), 8.02 (d, 1H, J = 4.4 Hz, Ar-H), 8.05 (s, 1H, Ar-H), 8.08 (s, 1H, OH exchangeable by D$_2$O); MS (m/z): 397 (M$^{.+}$, 3.71%), 131 (100.0%); Anal.Calcd for C$_{20}$H$_{14}$F$_3$N$_5$O (397.35): C, 60.45; H, 3.55; N, 17.62; Found: C, 60.74; H, 3.52; N, 17.80%.

5-Methyl-3-((3-(trifluoromethyl)phenyl)diazenyl) pyrazolo[1,5-a]pyrimidine-2,7-diol (8a) and 5,6-Dimethyl-3-((3-(trifluoromethyl)phenyl)diazenyl)pyrazolo[1,5-a] pyrimidine-2,7-diol (8b)

A mixture of **4a** (2.71 g, 0.01 mol), ethyl acetoacetate, or ethyl methyl acetoacetate (0.01 mol) in acetic acid was heated under reflux for 8 h. The reaction mixture was cooled and the solid product was collected and crystallized from ethanol.

5-Methyl-3-((3-(trifluoromethyl)phenyl)diazenyl) pyrazolo[1,5-a]pyrimidine-2,7-diol (8a)

Yield: 67% as orange crystals; m.p.: 159-161 °C; IR: ν/cm^{-1}: 3313, 3179 (br. 2OH), 3077 (CH-aromatic), 2850 (CH-aliphatic), 1566 (N=N); ^{1}H NMR (400 MHz, DMSO-d_6) δ/ppm: 2.37 (s, 3H, CH$_3$), 5.94 (s, 1H, CH-pyrim.), 7.38–7.80 (m, 2H, Ar H), 8.03 (d, 1H, J = 7.2 Hz, Ar-H), 8.11 (s, 1H, Ar-H), 10.54, 12.85 (2 s, 2H, 2OH exchangeable by D$_2$O); ^{13}C NMR (100 MHz, CDCl$_3$) δ: 19.00 (CH$_3$), 119.53 (CF$_3$), 65.25, 150.30, 151.40 (3C-pyrazole), 110.00, 143.45, 160.00 (3C-pyrimidine), 120.00, 125.00, 125.54, 126.03, 130.32, 130.96 (Ar-C); MS (m/z): 337 (M$^{.+}$, 4.39%), 40 (100.0%); Anal.Calcd for C$_{14}$H$_{10}$F$_3$N$_5$O$_2$ (337.26): C, 49.86; H, 2.99; N, 20.77; Found: C, 50.08; H, 3.01; N, 21.04%.

5,6-Dimethyl-3-((3-(trifluoromethyl)phenyl)diazenyl) pyrazolo[1,5-a]pyrimidine-2,7-diol (8b)

Yield: 64% as orange crystals; m.p.: 172-174 °C; IR: ν/cm^{-1}: 3176 (br. OH), 3060 (CH-aromatic), 2840 (CH-aliphatic), 1566 (N=N); ^{1}H NMR (400 MHz, DMSO-d_6) δ/ppm: 2.00, 2.39 (2 s, 6H, 2CH$_3$), 5.94 (s, 1H, OH exchangeable by D$_2$O), 7.38 (d, 1H, J = 8 Hz, Ar-H), 7.56 (t, 1H, J = 12 Hz, Ar-H), 7.78 (d, 1H, J = 8.4 Hz, Ar-H), 8.02 (s, 1H, Ar-H), 10.53 (s,1H, OH exchangeable by D$_2$O);

MS (m/z): 351 (M$^{.+}$, 1.16%), 43 (100.0%); Anal.Calcd for C$_{15}$H$_{12}$F$_3$N$_5$O$_2$ (351.28): C, 51.29; H, 3.44; N, 19.94; Found: C, 51.52; H, 3.49; N, 20.17%.

7-Amino-2-hydroxy-5-aryl-3-((3-(trifluoromethyl)phenyl) diazenyl)pyrazolo[1,5-a]pyrimidines-6-carbonitrile (10a-c)

To a suspension of compound **4a** (2.71 g, 0.01 mol) and arylidene malononitriles (0.01 mol) in ethanol (30 mL), piperidine (0.5 mL) was added. The mixture was heated under reflux for 7 h and allowed to cool. The formed product was collected by filtration and crystallized from dioxane.

7-Amino-2-hydroxy-5-phenyl-3-((3-(trifluoromethyl)phenyl) diazenyl)pyrazolo[1,5-a]pyrimidine-6-carbonitrile (10a)

Yield: 68% as Brown crystals; m.p.: 289-291 °C; IR: ν/cm^{-1}: 3388 (br. NH$_2$ & OH), 3064 (CH-aromatic), 2217 (C≡N), 1632 (C=N), 1534 (N=N); ^{1}H NMR (400 MHz, DMSO-d_6) δ/ppm: 7.53-7.57 (m, 4H, Ar-H), 7.71 (d, 1H, J = 5.6 Hz, Ar-H), 7.85 (d, 2H, J = 8 Hz, Ar-H), 8.05 (t, 1H, J = 2.8 Hz, Ar-H), 8.16 (s, 1H, Ar-H), 8.91 (s, 3H, OH & NH$_2$ exchangeable by D$_2$O); MS (m/z): 423 (M$^{.+}$, 16.03%), 40 (100.0%); Anal.Calcd for C$_{20}$H$_{12}$F$_3$N$_7$O (423.35): C, 56.74; H, 2.86; N, 23.16; Found: C, 57.01; H, 2.83; N, 23.41%.

7-Amino-2-hydroxy-5-p-tolyl-3-((3-(trifluoromethyl)phenyl) diazenyl)pyra-zolo[1,5-a]pyrimid-ine-6-carbonitrile (10b)

Yield: 77% as Brown crystals; m.p.: 299-301 °C; IR: ν/cm^{-1}: 3336, 3125 (OH & NH$_2$), 3050 (CH-aromatic), 2860 (CH-aliphatic), 2214 (C≡N), 1632 (C=N), 1539 (N=N); ^{1}H NMR (400 MHz, DMSO-d_6) δ/ppm: 2.39 (s, 3H, CH$_3$), 5.95 (s, 2H, NH$_2$ exchangeable by D$_2$O), 7.33-7.96 (m, 6H, Ar-H), 8.04 (d, 1H, J = 4.4 Hz, Ar-H), 8.14 (s, 1H, Ar-H), 10.54 (s, 1H, OH exchangeable by D$_2$O); ^{13}C NMR (100 MHz, DMSO-d_6) δ: 21.46 (CH$_3$), 116.23 (C≡N), 124.83 (CF$_3$) 77.51, 117.28, 118.09, 123.14, 125.85, 129.16, 129.41, 130.32, 130.97, 134.52, 141.01, 144.90, 149.86, 152.12, 161.23, 162.48 (Ar-C); MS (m/z): 437 (M$^{.+}$, 21.96%), 40 (100.0%); Anal.Calcd for C$_{21}$H$_{14}$F$_3$N$_7$O (437.38): C, 57.67; H, 3.23; N, 22.42; Found: C, 57.89; H, 3.30; N, 22.67%.

7-Amino-2-hydroxy-5-(4-methoxyphenyl)-3-((3-(trifluoromethyl)phenyl)diazenyl)pyrazolo[1,5-a]-pyrimidine-6-carbonitrile (10c)

Yield: 67% as **Brown** crystals; m.p.: 293-295 °C; IR: ν/cm^{-1}: 3343 (br. OH & NH$_2$), 3089 (CH-aromatic), 2860 (CH-aliphatic), 2212 (C≡N), 1610 (C=N), 1538 (N=N);

^{1}H NMR (400 MHz, DMSO-d_6) δ/ppm: 3.84 (s, 3H, OCH_3), 7.10 (d, 3H, $J = 8.8$ Hz, Ar-H), 7.71 (d, 1H, $J = 5.6$ Hz, Ar-H), 7.88 (d, 2H, $J = 8.8$ Hz, Ar-H), 8.05 (t, 1H, $J = 8.8$ Hz, Ar-H), 8.15 (s, 1H, Ar-H), 8.80 (s, 3H, NH_2 & OH exchangeable by D_2O); MS (m/z): 453 (M·+, 17.30%), 308 (100.0%); Anal.Calcd for $C_{21}H_{14}F_3N_7O_2$ (453.38): C, 55.63; H, 3.11; N, 21.63; Found: C, 55.89; H, 3.14; N, 21.88%.

Ethyl 7-amino-2-hydroxy-5-p-tolyl-3-((3-(trifluoromethyl)phenyl)diazenyl)pyrazolo[1,5-a]pyrim-idine-6-carboxylate (11a) and ethyl 7-amino-2-hydroxy-5-(4-methoxyphenyl)-3-((3-(trifluoro-methyl)phenyl)diazenyl)pyrazolo[1,5-a]pyrimidine-6-carboxylate (11b)

A mixture of compound **4a** (2.71 g, 0.01 mol) and arylidenecyanoacetate (0.01 mol) in ethanol (30 mL) was treated with piperidine (0.5 mL). The mixture was heated under reflux for 10 h., and allowed to cool. The formed product was collected by filtration and crystallized from dioxane.

Ethyl 7-amino-2-hydroxy-5-p-tolyl-3-((3-(trifluoromethyl)phenyl)-diazenyl)pyrazolo[1,5-a]pyri-midine-6-carboxylate (11a)

Yield: 61% as red crystals; m.p.: 299-301 °C; IR: ν/cm^{-1}: 3427, 3308 (OH & NH_2), 3060 (CH-aromatic), 2989 (CH-aliphatic), 1680 (C=O), 1614 (C=N), 1534 (N=N); ^{1}H NMR (400 MHz, DMSO-d_6) δ/ppm: 0.89 (t, 3H, $CH_2\underline{CH_3}$), 2.36 (s, 3H, CH_3), 4.00 (q, 2H, $\underline{CH_2}CH_3$), 7.26 (d, 3H, $J = 8$ Hz, Ar-H), 7.39 (d, 1H, $J = 7.6$ Hz, Ar-H), 7.67 (d, 2H, $J = 9.6$ Hz, Ar-H), 8.00 (t, 1H, $J = 7.6$ Hz, Ar-H), 8.08 (s, 1H, Ar-H), 8.30 (s, 3H, NH_2 & OH exchangeable by D_2O); ^{13}C NMR (100 MHz, DMSO-d_6) δ: 13.66 ($CH_2\underline{CH_3}$), 21.38 (CH_3), 56.46 (CH_3), 124.66 (CF_3), 166.18 (CO), 61.55, 147.41, 147.44 (3C-pyrazole), 116.76, 139.29, 162.09 (3C-pyrimidine), 118.89, 123.09, 123.80, 128.60, 128.95, 130.75, 131.09, 136.97, 137.44, 161.80 (Ar-C); MS (m/z): 484 (M·+, 54.24%), 143 (100.0%); Anal.Calcd for $C_{23}H_{19}F_3N_6O_3$ (484.43): C, 57.02; H, 3.95; N, 17.35; Found: C, 57.13; H, 4.02; N, 17.59%.

Ethyl 7-amino-2-hydroxy-5-(4-methoxyphenyl)-3-((3-(trifluoromethyl)-phenyl)diazenyl)pyrazolo-[1,5-a]pyrimidine-6-carboxylate (11b)

Yield: 69% as red crystals; m.p.: 222-224 °C; IR: ν/cm^{-1}: 3409, 3310, 3189 (OH & NH_2), 3040 (CH-aromatic), 2811 (CH-aliphatic), 1680 (C=O), 1610 (C=N), 1570 (N=N); ^{1}H NMR (400 MHz, DMSO-d_6) δ/ppm: 1.26 (t, 3H, $CH_2\underline{CH_3}$), 3.85 (s, 3H, OCH_3), 4.25 (q, 2H,

$\underline{CH_2}CH_3$), 5.92 (s, 2H, NH_2 exchangeable by D_2O), 7.01 (d, 1H, $J = 8.8$ Hz, Ar-H), 7.38 (d, 2H, $J = 7.6$ Hz, Ar-H), 7.54 (t, 1H, $J = 8$ Hz Ar-H), 7.77 (d, 1H, $J = 8$ Hz, Ar-H), 8.05 (d, 2H, $J = 8.4$ Hz, Ar-H), 8.29 (s, 1H, Ar-H), 10.52 (s,1H, OH exchangeable by D_2O); MS (m/z): 500 (M·+, 1.96%), 92 (100.0%); Anal.Calcd for $C_{23}H_{19}F_3N_6O_4$ (500.43): C, 55.20; H, 3.83; N, 16.79; Found: C, 55.41; H, 3.90; N, 16.98%.

Biological activities

Cell lines

The American Type Culture Collection provided hepatocellular (HepG-2), human colon (HCT-116), and breast (HepG-2) cancer cells (ATCC, Rockville, MD, USA). The cells were cultured in RPMI-1640 media with 10% inactivated fetal calf serum and 50 µg/mL gentamycin supplementation. The cells were kept at 37 degrees Celsius in a humidified environment with 5% CO_2.

In vitro Anti-tumor activity assessment using MTT assay

The MTT test was used in triplicate to assess the viability of control and treatment cells. Yellow MTT [3-(4,5-dimethylthiazol-2-yl)-2,5-diphenyltetrazolium bromide, a tetrazole] was converted to purple formazan in the mitochondria of live cells in the MTT assay, a standard colorimetric assay (an assay that evaluates color changes) for evaluating cellular growth. To dissolve the insoluble purple formazan product into a colored solution, a solubilizing solution of dimethyl sulfoxide (DMSO) was added. Three tumor cell lines were seeded at a density of 1104 cells/well in 96-well plates containing 100 µL of the growth media. Cells could adhere for 24 h until confluence, then washed with PBS before being treated with various concentrations of chemicals in a fresh maintenance medium ranging from 50 to 1.56 µg and incubated for 24 h at 37 degrees Celsius. In the absence of test substances, untreated cells were used as a control. As a negative control, cells that had not been treated were employed. Using a multichannel pipette, serial twofold dilutions of the tested compounds were applied to a 96-well tissue culture plate (Eppendorf, Germany). The culture supernatant was replaced with fresh media after treatment (24 h). The cells in each well were then treated for 4 h at 37 °C with 100 µL of MTT solution (5 mg/mL). The MTT solution was withdrawn once the incubation period was completed, and 100 µL of DMSO was added to each well. A microplate reader was used to measure the absorbance at 570 nm (SunRise TECAN, Inc, USA). The absorbance of untreated cells was assumed to be 100%. Three different experiments were used to determine the results [60, 67].

Data analysis The percentage of cell viability was computed as [1(ODt/ODc)] 100 percent, where ODt represents the mean optical density of wells treated with the tested substance and ODc represents the mean optical density of untreated cells. The IC_{50} value, which is the concentration of an individual chemical that causes 50 percent cell death, was calculated from graphical plots of surviving cells vs compound concentrations.

Apoptosis detection studies

Determination of the active Caspase-3 With an active Quantikine-Human Caspase-3 Immunoassay, the manufacturer's technique estimated the active level of Caspase-3 (R&D Systems, Inc. Minneapolis, USA). The cells were collected and lysed after being washed in PBS and added to the protease inhibitor extraction buffer (1 mL per 1×10^7 cells).

Before the test, the lysate was diluted immediately. Finally, the optical density of each well was calculated in 30 min using a microplate reader set to 450 nm [68].

Determination of mitochondrial apoptosis pathway proteins BAX and Bcl-2 The compounds were stimulated for the BAX or Bcl-2 test, and the cell extraction buffer was lysed. Cells were extracted from the American Culture Set, cultured in RPMI 1640 with 10% fetal serum from bovine animals at 37 °C, and the compounds were stimulated for the BAX or Bcl-2 test. In Regular Diluent Buffer, this lysate was diluted across the test range and analyzed for human active BAX or Bcl-2 content. (Cells are plated at a density of 1.2–1.8 10,000 cells per well in a volume of 100 μL complete growth medium + 100 uL of the tested chemical per well in a 96-well plate for 24 hours before being measured for human active BAX or Bcl-2) [68].

Cell cycle analysis

HepG-2 cancer cells were planted into a 6-well plate at a concentration of 1×10^5 cells per well and incubated for 24 h. For 24 h, cells were treated with either a vehicle (0.1 percent DMSO) or compound **8b**. After that, cells were collected and fixed for 12 h in ice-cold 70% ethanol at 4 °C. Ethanol and cold PBS are removed from the cells and incubated for 30 min at 37 °C in 0.5 mL PBS containing 1 mg/mL Rnase. For around 30 min, the cells were stained with propidium iodide in the dark. The flow cytometer was then used to determine the DNA content.

Annexin V-FITC assay

The cancer cells of HepG-2 were plated in a 6-well plate, incubated for 24 h, and then treated for another 24 h with either a vehicle (0.1 percent DMSO) or the tested compounds. Harvesting cells, washing them with PBS, and spraying them in the dark with Annexin V-FITC and propidium iodide (PI) were all done in the binding buffer (10 mM HEPES, 140 mM NaCl, and 2.5 mM $CaCl_2$ at pH 7.4). After that, the flow cytometer was examined [68].

EGFR assay

The inhibitory activity of the most promising chemicals on HepG-2 cells was tested using the same instructions and the protocol producer's documented approach against $EGFR^{wt}$ and EGFR $^{L858R-TK}$ [24].

In silico physicochemical and ADME properties prediction

The molecular structures were translated to SMILES using Chemdraw 19.0. SMILS were subsequently added to the Swiss ADME website for physicochemical characteristics, lipophilicity, pharmacokinetics, ADME parameters, and medicinal chemistry friendliness measurement [69–71].

Molecular docking

The computational program and docking method were performed as described in previous work [72, 73] utilizing Molecular Operating Environment software 14.0901 (MOE), Chemical Computing Group Inc., Montreal, Quebec, Canada. The enzyme (1M17) was taken from the protein data bank, the water molecule was removed, all hydrogen atoms were added, then the enzyme was polished, and the energy was minimized using MOE. The Erlotinib was redocked into the EGFR binding site using the MOE software default option to ensure the protein was ready for docking. The target hybrids were created in chem draw, then transferred to MOE, where it was protonated in three dimensions, hidden hydrogen rendered, and energy minimized before being saved as a mdb for docking into the active site. The docking procedure was then carried out using the default protocol.

Compliance with ethical standards

References

1. Ali I, Wani WA, Haque A, Saleem K. "Glutamic acid and its derivatives: candidates for rational design of anticancer drugs,". Future Medicinal Chem. 2013;5:961–78.

2. Ali I, Wani WA, Saleem K, Wesselinova D. "Syntheses, DNA binding and anticancer profiles of L-glutamic acid ligand and its copper (II) and ruthenium (III) complexes. Medicinal Chem. 2013;9:11–21.

3. Hussain A, Ovesb M, Alajmi MF, Hussainc I, Amird S, Ahmede J, et al. "Biogenesis of ZnO nanoparticles using Pandanus odorifer leaf extract: anticancer and antimicrobial activities,". RSC Adv. 2019;9:15357–69.

4. Shamroukh AH, El-Shahat M, Drabowicz J, Ali MM, Rashad AE, Ali HS. "Anticancer evaluation of some newly synthesized N-nicotinonitrile derivative,". Eur J Medicinal Chem. 2013;69:521–6.

5. Ali I, Wani WA, Khan A, Haque A, Ahmad A, Saleem K, et al. "Synthesis and synergistic antifungal activities of a pyrazoline based ligand and its copper (II) and nickel (II) complexes with conventional antifungals,". Microb Pathogenesis. 2012;53:66–73.

6. Ali I, Wani WA, Saleem K, Hsieh M-F. "Anticancer metallodrugs of glutamic acid sulphonamides: in silico, DNA binding, hemolysis and anticancer studies,". RSC Adv. 2014;4:29629–41.

7. Ali I, Wani WA, Saleem K, Haque A. "Thalidomide: A banned drug resurged into future anticancer drug. Curr Drug Ther. 2012;7:13–23.

8. Mohammad RM, Muqbil I, Lowe L, Yedjou C, Hsu H, Lin L, et al. "Broad targeting of resistance to apoptosis in cancer," in. Semin Cancer Biol. 2015;35:S78–S103.

9. Findley HW, Gu L, Yeager AM, Zhou M. "Expression and regulation of Bcl-2, Bcl-xl, and Bax correlate with p53 status and sensitivity to apoptosis in childhood acute lymphoblastic leukemia,". Blood, J Am Soc Hematol. 1997;89:2986–93.

10. Harun SNA, Israf DA, Tham CL, Lam KW, Cheema MS, Md Hashim NF. "The molecular targets and anti-invasive effects of 2, 6-*bis*-(4-hydroxyl-3methoxybenzylidine) cyclohexanone or BHMC in MDA-MB-231 human breast cancer cells,". Molecules. 2018;23:865.

11. Hassan M, Watari H, AbuAlmaaty A, Ohba Y, Sakuragi N, "Apoptosis and molecular targeting therapy in cancer," BioMed Res. Int. 2014;2014:150845.

12. Wang A, Zhang Y, Cao P. "Inhibition of BAP31 expression inhibits cervical cancer progression by suppressing metastasis and inducing intrinsic and extrinsic apoptosis,". Biochem. Biophys Res Commun. 2019;508:499–506.

13. Westphal D, Dewson G, Czabotar PE, Kluck RM. "Molecular biology of Bax and Bak activation and action,". Biochimica et Biophysica Acta (BBA)-Mol Cell Res. 2011;1813:521–31.

14. D'Orsi B, Mateyka J, Prehn JH. "Control of mitochondrial physiology and cell death by the Bcl-2 family proteins Bax and Bok,". Neurochemistry Int. 2017;109:162–70.

15. Cotter TG. "Apoptosis and cancer: the genesis of a research field,". Nat Rev Cancer. 2009;9:501–7.

16. Watson A. "Apoptosis and colorectal cancer,". Gut. 2004;53:1701–9.

17. Fathy U, Abd El Salam HA, Fayed EA, Elgamal AM, Gouda A. "Facile synthesis and *in vitro* anticancer evaluation of a new series of tetrahydroquinoline,". Heliyon. 2021;7:e08117.

18. Ammar YA, Elhagali GAM, Abusaif MS, Selim MR, Zahran MA, Naser T, et al. "Carboxamide appended quinoline moieties as potential anti-proliferative agents, apoptotic inducers and Pim-1 kinase inhibitors,". Medicinal Chem Res. 2021;30:1649–68.

19. Fayed EA, Gohar NA, Farrag AM, Ammar YA. "Upregulation of BAX and caspase-3, as well as downregulation of Bcl-2 during treatment with indeno [1, 2-*b*] quinoxalin derivatives, mediated apoptosis in human cancer cells," Archiv der Pharm. 2022;355: e2100454.

20. Pollard TD, Earnshaw W, Schwartz J "Programmed cell death," *Cell biology. 2nd ed. Phiadelphia: Saunders-Elsevier*, 2008.

21. Narisawa T, Fukaura Y, Yazawa K, Ishikawa C, Isoda Y, Nishizawa Y. "Colon cancer prevention with a small amount of dietary perilla oil high in alpha-linolenic acid in an animal model,". Cancer. 1994;73:2069–75.

22. Bogdał MN, Hat B, Kochańczyk M, Lipniacki T. "Levels of pro-apoptotic regulator Bad and anti-apoptotic regulator Bcl-xL determine the type of the apoptotic logic gate,". BMC Syst Biol. 2013;7:1–17.

23. Fayed EA, Sabour R, Harras MF, Mehany A. "Design, synthesis, biological evaluation and molecular modeling of new coumarin derivatives as potent anticancer agents,". Medicinal Chem Res. 2019;28:1284–97.

24. Fayed EA, Eldin RRE, Mehany A, Bayoumi AH, Ammar YA. "Isatin-Schiff's base and chalcone hybrids as chemically apoptotic inducers and EGFR inhibitors; design, synthesis, anti-proliferative activities and in silico evaluation,". J Mol Struct. 2021;1234:130159.

25. Fayed EA, Ammar YA, Saleh MA, Bayoumi AH, Belal A, Mehany AB, et al. "Design, synthesis, antiproliferative evaluation, and molecular docking study of new quinoxaline derivatives as apoptotic inducers and EGFR inhibitors,". J Mol Struct. 2021;1236;130317.

26. Unger C. "New therapeutic approaches in cancer treatment,". Drugs Future. 1997;22:1337–45. pp.

27. Ullah MF, Khan MW. "Food as medicine: potential therapeutic tendencies of plant derived polyphenolic compounds,". Asian Pac J Cancer Prev. 2008;9:187–96.

28. Hoyun L, Solomon V, Changkun H. "Hybrid pharmacophore design and synthesis of isatin–Chemistry,". Bioorg Med Chem. 2009;17:7585–92.

29. Selleri S, Bruni F, Costagli C, Costanzo A, Guerrini G, Ciciani G, et al. "A novel selective GABAA α1 receptor agonist displaying sedative and anxiolytic-like properties in rodents,". J medicinal Chem. 2005;48:6756–60.

30. Metwally NH, Abdallah MA, Almabrook SA. "Pyrazolo [1, 5-*a*] Pyrimidine Derivative as Precursor for Some Novel Pyrazolo [1, 5-*a*] Pyrimidines and Tetraheterocyclic Compounds,". J Heterocycl Chem. 2017;54:347–54.

31. Ajeesh Kumar A, Nair KB, Bodke YD, Sambasivam G, Bhat KG. "Design, synthesis, and evaluation of the anticancer properties of a novel series of carboxamides, sulfonamides, ureas, and thioureas derived from 1, 2, 4-oxadiazol-3-ylmethyl-piperazin-1-yl substituted with pyrazolo [1, 5-*a*] pyrimidine derivatives,". Monatshefte für Chem-Chem Monthly. 2016;147:2221–34.

32. Selleri S, Bruni F, Costagli C, Costanzo A, Guerrini G, Ciciani G, et al. "2-Arylpyrazolo [1, 5-*a*] pyrimidin-3-yl acetamides. New potent and selective peripheral benzodiazepine receptor ligands,". Bioorg Medicinal Chem. 2001;9:2661–71.

33. Kumar S, Narasimhan B. "Therapeutic potential of heterocyclic pyrimidine scaffolds,". Chem Cent J. 2018;12:1–29.

34. El Shehry MF, Ghorab MM, Abbas SY, Fayed EA, Shedid SA, Ammar YA. "Quinoline derivatives bearing pyrazole moiety: Synthesis and biological evaluation as possible antibacterial and antifungal agents,". Eur J Med Chem. 2018;143;1463–73.

35. Hussein MA. "Synthesis, anti-inflammatory, and structure antioxidant activity relationship of novel 4-quinazoline,". Medicinal Chem Res. 2013;22:4641–53.

36. Chimichi S, Boccalini M, Selleri S, Costagli C, Guerrini G, Viola G. "On the reactivity of 6-acetyl-7-(2-dimethylaminovinyl) pyrazolo [1, 5-a] pyrimidines with 1, 3-and 1, 4-bisnucleophiles,". Org Biomolecular Chem. 2008;6:739–44.

37. Taliani S, Pugliesi I, Barresi E, Salerno S, Marchand C, Agama K, et al. "Phenylpyrazolo [1, 5-a] quinazolin-5 (4 H)-one: A Suitable Scaffold for the Development of Noncamptothecin Topoisomerase I (Top1) Inhibitors,". J Medicinal Chem. 2013;56:7458–62.

38. Shekarrao K, Kaishap PP, Saddanapu V, Addlagatta A, Gogoi S, Boruah RC. "Microwave-assisted palladium mediated efficient synthesis of pyrazolo [3, 4-b] pyridines, pyrazolo [3, 4-b] quinolines, pyrazolo [1, 5-a] pyrimidines and pyrazolo [1, 5-a] quinazolines,". RSC Adv. 2014;4:24001–6.

39. Flefel EM, El-Sofany WI, El-Shahat M, Naqvi A, Assirey E. "Synthesis, molecular docking and in vitro screening of some newly synthesized triazolopyridine, pyridotriazine and pyridine–pyrazole hybrid derivatives,". Molecules. 2018;23:2548.

40. Flefel E, Salama M, El-Shahat M, El-Hashash M, El-Farargy A. "A novel synthesis of some new pyrimidine and thiazolopyrimidine derivatives for anticancer evaluation,". Phosphorus, Sulfur, Silicon Relat Elem. 2007;182:1739–56.

41. Rashad AE, Shamroukh AH, Yousif NM, Salama MA, Ali HS, Ali MM, et al. "New pyrimidinone and fused pyrimidinone derivatives as potential anticancer chemotherapeutics,". Arch der Pharmazie. 2012;345:729–38.

42. Deshmukh S, Dingore K, Gaikwad V, Jachak M. "An efficient synthesis of pyrazolo [1, 5-a] pyrimidines and evaluation of their antimicrobial activity,". J Chem Sci. 2016;128:1459–68.

43. Fadeyi OO, Okoro CO. "Synthesis of 5-(trifluoromethyl) cyclohexane-1, 3-dione and 3-amino-5-(trifluoromethyl) cyclohex-2-en-1-one: new trifluoromethyl building block,". Tetrahedron Lett. 2008;49:4725–7.

44. Singh RP, Jean'ne MS. "Nucleophilic trifluoromethylation reactions of organic compounds with (trifluoromethyl) trimethylsilane,". Tetrahedron. 2000;39:7613–32.

45. Ranatunge RR, EarlDavid RA, David SG, Janero R, Allison GL, Madhavi MM, et al. "3-(2-Methoxytetrahydrofuran-2-yl) pyrazoles: a novel class of potent, selective cyclooxygenase-2 (COX-2) inhibitors,". Bioorg Medicinal Chem Lett. 2004;14:6049–52.

46. Sridhar R, Perumal PT, Etti S, Shanmugam G, Ponnuswamy MN, Prabavathy VR, et al. "Design, synthesis and anti-microbial activity of 1H-pyrazole carboxylates,". Bioorg medicinal Chem Lett. 2004;14:6035–40.

47. Hu H, Ge C, Ding L, Zhang A. Synthesis of Novel 1-[(2, 6-Dichloro-4-trifluoromethyl) phenyl]-3-aryl-1H-pyrazole-4-carbaldehydes. Molecules. 2010;15:7472–8..

48. Aggarwal R, Kumar R, Kumar S, Garg G, Mahajan R, Sharma J. "Synthesis and antibacterial activity of some 5-hydroxy-5-trifluoromethyl-4, 5-dihydropyrazol-1-thiocarboxamides, 3-trifluoromethylpyrazol-1-thiocarboxamides and 4-aryl-2-(5 (3)-trifluoromethyl-1-pyrazolyl) thiazoles,". J Fluor Chem. 2011;132:965–72.

49. Jeschke P. "The unique role of halogen substituents in the design of modern agrochemicals,". Pest Manag Sci: Former Pestic Sci. 2010;66:10–27.

50. Aggarwal R, Bansal A, Mittal A. "Synthesis and antimicrobial activity of 3-(2-thienyl)-4-arylazo-5-hydroxy-5-trifluoromethyl-Δ2-isoxazolines and 3-(2-thienyl)-4-arylazo-5-trifluoromethylisoxazoles,". J Fluor Chem. 2013;145:95–101.

51. Flefel EM, El-Sofany WI, Al-Harbi RA, El-Shahat M. "Development of a novel series of anticancer and antidiabetic: spirothiazolidines analogs,". Molecules. 2019;24:2511.

52. El-Shahat M, El-Sofany WI, Soliman A-GA, Hasanin M. "Newly synthesized imidazolotriazole, imidazolotriazine, and imidazolepyrazole hybrid derivatives as promising antimicrobial agents,". J Mol Struct. 2022;1250:131727.

53. AbdelFattah BA, Khalifa MMA, El-Sehrawi H, Fayed E, Bayoumi A, Said M. "Synthesis and anxiolytic activity of some novel 5-oxo-1, 4-oxazepine derivatives,". Lett Drug Des Discov. 2011;8:330–8.

54. Fayed E, Ahmed H. "Synthesis, characterization and pharmacological evaluation of some new 1, 4-diazepine derivatives as anticancer agents,". Der Pharma Chem. 2016;8:77–90.

55. Ammar Y, Fayed E, Bayoumi A, Saleh M. "Synthesis and biological evaluation of new amides pro-drugs containing naproxen moiety as anti-inflammatory and antimicrobial agents,". Der Pharma Chem. 2016;8:495–508.

56. El-Kalyoubi SA, Fayed EA, Abdel-Razek AS, "Erratum: One pot synthesis, antimicrobial and antioxidant activities of fused uracils: Pyrimidodiazepines, lumazines, triazolouracil and xanthines." Chem Cent J. 2017;11:69. https://doi.org/10.1186/s13065-017-0294-0.

57. Fayed EA, Ebrahim MA, Fathy U, El Saeed HS, Khalaf WS. "Evaluation of quinoxaline derivatives as potential ergosterol biosynthesis inhibitors: design, synthesis, ADMET, molecular docking studies, and antifungal activities,". J Mol Struct. 2022;1267:133578.

58. El-Shahat M, Salama M, El-Farargy AF, Ali MM, Ahmed DM. "Effective pharmacophore for CDC25 phosphatases enzyme inhibitors: newly synthesized bromothiazolopyrimidine derivatives,". Mini Rev Medicinal Chem. 2021;21:118–31.

59. El-Sofany WI, El-sayed WA, Abd-Rabou AA, El-Shahat M. "Synthesis of new imidazole-triazole-glycoside hybrids as anti-breast cancer candidates,". J Mol Struct. 2022;1270:133942.

60. Fayed EA, Eissa SI, Bayoumi AH, Gohar NA, Mehany A, Ammar YA. "Design, synthesis, cytotoxicity and molecular modeling studies of some novel fluorinated pyrazole-based heterocycles as anticancer and apoptosis-inducing agents,". Mol diversity. 2019;23:165–81.

61. Zhang TSDZ, Wang S, Shafeev M. "Pyrazole Compounds," (in English). Pat Appl 2002;436:915 B1.

62. Lipinski CA, Lombardo F, Dominy BW, Feeney PJ. "Experimental and computational approaches to estimate solubility and permeability in drug discovery and development settings,". Adv drug Deliv Rev. 1997;23:3–25.

63. Ghose AK, Viswanadhan VN, Wendoloski JJ. "Prediction of hydrophobic (lipophilic) properties of small organic molecules using fragmental methods: an analysis of ALOGP and CLOGP methods,". J Phys Chem A. 1998;102:3762–72.

64. Veber DF, Johnson SR, Cheng H-Y, Smith BR, Ward KW, Kopple KD. "Molecular properties that influence the oral bioavailability of drug candidates,". J medicinal Chem. 2002;45:2615–23.

65. Egan WJ, Lauri G. "Prediction of intestinal permeability,". Adv drug Deliv Rev. 2002;54:273–89.

66. Muegge I, Heald SL, Brittelli D. "Simple selection criteria for drug-like chemical matter,". J medicinal Chem. 2001;44:1841–6.

67. Othman EM, Fayed EA, Husseiny EM, Abulkhair HS. "Apoptosis induction, PARP-1 inhibition, and cell cycle analysis of leukemia cancer cells treated with novel synthetic 1, 2, 3-triazole-chalcone conjugates,". Bioorg Chem. 2022;123:105762.

68. Fayed EA, Ammar YA, Ragab A, Gohar NA, Mehany AB, Farrag AM. "In vitro cytotoxic activity of thiazole-indenoquinoxaline hybrids as apoptotic agents, design, synthesis, physicochemical and pharmacokinetic studies,". Bioorg Chem. 2020;100:103951.

69. Fayed EA, Bayoumi AH, Saleh AS, Al-Arab EME, Ammar YA. "In vivo and in vitro anti-inflammatory, antipyretic and ulcerogenic activities of pyridone and chromenopyridone derivatives, physicochemical and pharmacokinetic studies,". Bioorg Chem. 2021;109:104742.

70. Fayed EA, Nosseir ES, Atef A, El-Kalyoubi SA. In vitro antimicrobial evaluation and in silico studies of coumarin derivatives tagged with pyrano-pyridine and pyrano-pyrimidine moieties as DNA gyrase inhibitors. Mol Divers. 2022;26:341–63.

71. Fayed EA, Al-Arab EME, Saleh AS, Bayoumi AH, Ammar YA. "Design, synthesis, in silico studies, in vivo and in vitro assessment of pyridones and thiazolidinones as anti-inflammatory, antipyretic and ulcerogenic hits,". J Mol Struct. 2022;1260:132839.

72. El-Kalyoubi SA, Ragab A, Abu Ali OA, Ammar YA, Seadawy MG, Ahmed A, et al. "One-Pot Synthesis and Molecular Modeling Studies of New Bioactive Spiro-Oxindoles Based on Uracil Derivatives as SARS-CoV-2 Inhibitors Targeting RNA Polymerase and Spike Glycoprotein,". Pharmaceuticals. 2022;15:376.

73. Desouky SE, Abu-Elghait M, Fayed EA, Selim S, Yousuf B, Igarashi Y, et al. "Secondary Metabolites of Actinomycetales as Potent Quorum Sensing Inhibitors Targeting Gram-Positive Pathogens: In Vitro and In Silico Study,". Metabolites. 2022;12:246.